Title

Mathematical modeling of IL-2 dysregulation in the pathogenesis of autoimmune disease

Author

Anzules, Jonathan Michael

Publication Date

2023

Mathematical modeling of IL-2 dysregulation in the pathogenesis of autoimmune disease

UNIVERSITY OF CALIFORNIA, MERCED

A dissertation submitted in partial satisfaction of the
requirements for the degree of

Doctor of Philosophy in
Quantitative and Systems Biology

Jonathan Michael Anzules

Committee in charge:

Professor Justin Yeakel, Chair
Professor Jennifer Manilay, Member
Professor Suzanne Sindi, Advisor
Professor Katrina Hoyer, Advisor

The Dissertation of Jonathan Michael Anzules is approved, and it is acceptable in quality and form for publication on microfilm and electronically.

_____

Jennifer Manilay

_____

Suzanne Sindi

_____

Katrina Hoyer

_____

Justin Yeakel, Chair

University of California, Merced

2022

DEDICATION

Esta disertación está dedicada a mi madre, Martha Anzules,
Ella se sacrificó tanto por el porvenir de sus hijos.

TABLE OF CONTENTS

Contents

LIST OF NOTATIONS AND ABBREVIATIONS

1. Antigen presenting cells (APC)
2. Aplastic anemia (AA)
3. Autoimmune Hemolytic Anemia (AIHA)
4. Autoimmune disease (AD)
5. CD8 cytotoxic T lymphocytes (CTL)
6. Dendritic cells (DC)
7. IL-2 knockout (IL-2 KO)
8. Natural Killer cells (NK)
9. Nonobese diabetic (NOD)
10. Physiological based pharmacokinetic modeling and simulation (PBPK)
11. Red blood cells (RBC)
12. Regulatory T cells; Tregs
13. Systemic lupus erythematosus; SLE
14. T cell receptor (TCR)
15. Type 1 diabetes(T1D)
16. Wild Type (WT)

PARAMETERS

Thymus production:

17. $\boldsymbol{\mu}\left(\frac{cell}{hour}\right)$: Naive T cell production rate from thymus
18. $\boldsymbol{\alpha}\left(\frac{cell}{hour}\right)$: Treg production rate from thymus
19. nK (*cells*): Carrying capacity of naive T cells
20. rK (*cells*): Carrying capacity of Tregs

Self-replication rates:

21. $S_N\left(\frac{1}{hour}\right)$: Naive T cell self replication rate
22. $S_T\left(\frac{1}{hour}\right)$: Activated T cell self replication rate
23. $S_R\left(\frac{1}{hour}\right)$: Treg self replication rate

Naive T cell differentiation rates:

24. $c\left(\frac{1}{hour}\right)$: Naive differentiation to Tregs
25. $\boldsymbol{\beta}\left(\frac{1}{hour}\right)$: Naive activation to activated T cells

Suppression dynamics:

26. n (unitless): Hill coefficient
27. K_A (*cells*): Treg half saturation rate for suppression of activation ($\boldsymbol{\beta}$)
28. K_i (*molecules*): IL-2 50% maximal response for activation suppression
29. $j\left(\frac{1}{cells}\right)$: Deactivation rate of activated T cells by Tregs
30. K_j (*molecules)*: IL-2 50% maximal response for activated T cell deactivation
31. K_B (*molecules*): IL-2 half saturation for suppression of Treg death rate

IL-2 cytokine expression and use:

32. p $\left(\frac{molecules}{cells \cdot hour}\right)$: T cell production rate of IL-2
33. e_T $\left(\frac{1}{cells \cdot hour}\right)$: Activated T cell consumption rate of IL-2
34. e_R $\left(\frac{1}{cells \cdot hour}\right)$: Tregs consumption rate of IL-2

Death rates:

35. d_N ($\frac{1}{hour}$): Naive T cell death rate
36. d_T $\left(\frac{1}{hour}\right)$: Activated T cell death rate
37. d_R $\left(\frac{1}{hour}\right)$: Treg death rate
38. d_T $\left(\frac{1}{hour}\right)$: IL-2 cytokine half life

LIST OF FIGURES

(teal). **(C)** Tregs and their subpopulations: Total Tregs (red), proliferating Tregs (green), naive/peripherally derived Tregs (teal), and thymic derived Tregs (purple).

Figure 8. Flow Diagram. Visual representation of our system of ordinary differential equations (equations 1 – 4). Solid line with arrows indicates the flow of cellular and cytokine populations while dashed lines with a bar head represent suppression. The system begins with the supply of naïve T cells and regulatory T cells (Tregs) by their production in the thymus. Naïve T cells differentiate into Tregs at rate $\boldsymbol{c}$ and can become activated T cells at rate β**.** Naive T cells, activated T cells, and Tregs have their own self replication rate (s_N, s_T, s_R) and death rate (d_N, d_T, d_R). IL-2 cytokine (produced by activated T cells at rate p) is consumed by Tregs at rate e_R and activated T cells at rate e_T. A, B, and C are terms that are influenced by the presence of IL-2 to inhibit the death rate of Tregs (d_R), inhibit naive T cell activation rate (β), and increase the deactivation rate of activated T cells (T). The only difference I have between WT and IL-2 KO simulation is the production rate of IL-2 (p). In the WT, p is set to be 1000 molecules per cell per hour, for the IL-2 KO model it is set to be 100 molecules per cell per hour.

Figure 9. Results from fmincon parameter estimation search. Each data point represents one resolution of my optimization algorithm (632 total). The x-axis represents the parameter value, while the y-axis represents the error value of each data point. The blue line in the scatter plot represents the line of best fit determined through linear regression analysis. The top right of each figure shows correlation value. **(A)** μ: thymic naïve T cell production rate **(B)** s_N: naïve T cell self-replication rate **(C)** β: naïve T cell activation rate **(C)** K_A: half suppression rate of naïve T cell activation rate.

Figure 10. Residuals and model output from representative parameter set. Each section of the figure contains the result of my simulation and comparison to the data (top) and the residuals of the model (bottom). The top figure contains the experimental results (black dots), the mean of data points (dotted line), and simulation results (solid black line). The bottom figure contains the residuals (black dots) and the 0 line (blue line). **(A-C)** WT data. **(D-F)** IL-2 KO data. **(A, D)** Total naïve T cells. **(C, E)** Total activated T cells. **(D, F)** Total Tregs.

Figure 11. Model fit to data and characterization of homeostatic expansion. All figures contain the results from data collection (black dots), mean of data (dotted line), and simulation results (solid line). **(A-B)** Each section is a table of figures for both WT (top row) and IL-2 KO (bottom row) data and simulation. For the simulation comparisons the WT is represented by a black line and the IL-2 KO by a dashed line. **(A)** Naive T cell population and its sub-populations, starting from the left each column represents the data for total naive T cells, proliferating naive T cells, and thymic derived naive T cells. **(B)** Activated T cell population and its sub-populations, starting from the left each column represents the data for total activated T cell count, proliferating activated T cells, naive derived activated T cells. **(C)** Tregs and their sub-populations, starting from the left each column represents total Treg counts, proliferating Tregs, thymic derived Tregs, naïve derived Tregs.

Figure 12. Comparison of Treg Population Dynamics in Wild-type and Knock-out Simulations: Total Tregs, Death Rate, and Proliferation Rates. Plots display the Log transformation of various Treg population rates and sizes. The solid lines indicate WT simulations, while the dotted lines reflect KO simulations. **(A)** Total Treg population size **(B)** Treg death rate and **(C)** Treg proliferation rate.

Figure 13. Results of μ sensitivity analysis. First order sensitivity analysis of +/- 10% LHS sampling of the **μ** parameter (thymic production rate of naive T cells). Results show the WT simulation. Blue dots represent experimental data, the top of the filled in area is the 90^{th} percentile result, while the bottom is the 10^{th} percentile mark, the blue line in the middle of the area represents the mean of all the model output.

Figure 14. Result of α sensitivity analysis. First order sensitivity analysis of +/- 90% of 3000 LHS sampling of parameter **α**, thymic production rate of Tregs. Results show the WT simulation. No filled in region is clearly seen (No variation).

Figure 15. Impact of IL-2 Deficiency on Treg Cell Dynamics: Dysregulation of the Treg populations. Results from the +/- 60% LHS sampling range of parameters: $\mathbf{d_R}$, **p**, $\mathbf{p_{KO}}$, $\mathbf{K_B}$; for 3000 simulations. Chosen parameters affect Treg survival. The shaded represents the range of variability across all simulation results, where the top line corresponds to the 90th percentile, representing the upper limit of the variability, and the bottom line corresponds to the 10th percentile, representing the lower limit of the variability. The solid lines within the shaded region represent the mean, which represents the average value across all simulations. Green represents the wild-type data, while pink represents the IL-2 KO data. **(A)** Available IL-2 cytokine in the system has a deterministic influence on **(B)** Treg death suppression strength. **(C-E)** Below every plot is a zoomed-in view of the data above it. **(C-E)** Represents the instantaneous rates of Treg death **(C),** Treg proliferation**(D),** and total Treg population size **(E)**.

Figure 16. Model prediction and prevention of autoimmune disease. Results from the +/- 60% LHS sampling range of parameters: $\mathbf{K_A}$, $\mathbf{K_{AKO}}$, **j**, $\mathbf{j_{KO}}$, $\mathbf{d_R}$; for 3000 simulations. Parameters with the 'KO' subscript has been edited on the IL-2 KO version of the model to find the best methodology to prevent autoimmune disease. The top figures are activating naive T cells, mid: activation suppression strength, bottom: removed effector cell. I look at the simulation past the point where I have data (day 18) all the way until day 25. The shaded represents the range of variability across all simulation results, where the top line corresponds to the 90th percentile, representing the upper limit of the variability, and the bottom line corresponds to the 10th percentile, representing the lower limit of the variability. The solid lines within the shaded region represent the mean, which represents the average value across all simulations. **(A)** No change to any IL-2 specific parameters. **(B)** Parameter $\mathbf{j_{KO}}$ is increased by 300%. **(C)** Half rate suppression, K_{AKO} , is reduced by 83%; increasing the suppression strength of $\boldsymbol{\beta}$ in the IL-2 KO model by the same proportion.

LIST OF TABLES

ACKNOWLEDGEMENT

As a first-generation college student, I experienced several hurdles that I overcame with the guidance and support of my advisers, Katrina Hoyer and Suzanne Sindi. I want to convey my heartfelt gratitude for all they have done for me; their insight and encouragement have positively impacted my academic life and my personal growth. Likewise, I am grateful to my committee members, Jennifer Manilay and Justin Yeakel, for their valuable input and support as they guided me through my project's development.

I used to feel that scientific research was a solitary pursuit, but in retrospect, this was inaccurate. Throughout the years, I received a lot of help from many individuals that advanced my work through simple, casual conversations. Many of these chats and exchanges provided me with guidance and encouragement, which aided my growth as a scientist. I am immensely appreciative of the learning atmosphere that I was surrounded by. I could not have completed this project without the assistance of our diverse UC Merced community.

I want to thank my bench-side experimental friends and collaborators, Genevieve Mullins and Kristen Valentine, for their invaluable help during the testing procedure and collection of data. Susana Tejeda and Christi Turner for their support and input during my immunology writing.

Thank you to my mathematical and computation friends and collaborators, Amandeep Kaur and Fabian Santiago, for their invaluable input while developing a mathematical model. Lihong Zhao for helping me translate my ideas into scientific and mathematical writing. With their input, I was able to structure the model and test it properly.

Outside of UC Merced, I had so much support from people who believed in me, who were there for me when I needed them the most, and who I know will be there for me in the future. Melissa Eisner, James Eisner, and Benjamin St. Claire, thank you for your support, encouragement, and all the laughs we have had together. I want to thank my girlfriend Haley Paulissian in particular - we met during a challenging time for both of us. Through our mutual growth and dedication, we have overcome many obstacles together. I am so very proud of the person that she has become, and I could not have finished my Ph.D. without her support.

Finally, I want to express my gratitude to my mother, Martha Anzules, who has always believed in me even when I could not. She has been a fountain of life and wisdom and has pushed me to become a better person and scientist. She is the person I can always rely on to correct my thinking and point me in the right direction. I dedicate this dissertation to my mother, who has given me her endless love.

CURRICULUM VITAE

JONATHAN MICHAEL ANZULES

(646) 712-1764 ⋄ jonanzule@gmail.com
3221 Thorn Avenue ⋄ Merced, CA 95340
github.com/J-Anzules/

EDUCATION

University of California, Merced *December 2022*
Ph.D. Student
Quantitative and Systems Biology

Brooklyn College *May 2014*
Bachelors of Science Degree
Biology

INTRODUCTION

I am a computational biologist specializing in genomic/proteomic analysis, statistical, machine learning models, and numerical analysis. With the support of my bench-side experience, I am adept at communicating complex technical information to interdisciplinary experts and lay audiences to identify innovative solutions for complex problems.

DATA ANALYTICS SKILLS

Programming Languages	Python, R, Matlab, Bash, Perl
Software & Tools	PhiSpy, scikit-learn, PyTorch, HPC clusters, fmincon, lhsdesign, BLAST, EMBOSS, FastQC, samtools, Matplotlib, ggplot, Jupyter, Pandas, NumPy, SciPy, Limma-Voom, Inkscape
Organization Tools	Trello, Slack, Amazon Web Services

RESEARCH EXPERIENCE

The homeostatic dynamics important for the prevention of autoimmune disease are not wholly understood. Under the mentorship of Dr. Katrina Hoyer and Dr. Suzanne Sindi, I designed and tested a mathematical model that represents known features of immune homeostasis. *Expected publication date: December 2022.* github.com/J-Anzules/HomeostaticExpansion

Modeling Homeostatic Expansion in a Healthy and Autoimmune system

- Collected, analyzed and quantified immune cellular populations for model fitting
- Developed a system of ODEs to represent our system of interest and used ode15s to solve it
- Developed an optimization algorithm using fmincon to minimize the R Squared values calculated between simulation results and data collected
- Implemented a Latin Hypercube Sampling algorithm for sensitivity analysis
- Identified critical parameter space necessary for preventing autoimmune disease

EXPERIENCE

Lawrence Livermore National Lab May - August 2022
Proteomic and Genomic Data Scientist (Data Science Summer Institute)

- Curated a database of SARS-CoV-2 genomic data for further analysis by a transformer based machine learning model
- Developed a pipeline that can detect viral variants and predict protein function/fitness

· Coordinated with a team of 4 data scientists to train and implement a 3D-CNN model of protein interactions to identity antiviral candidates against SARS-CoV-2

PhageNet September 2021 - May 2022
Genomic Data Scientist

· Implemented a machine learning based pipeline in Python, Perl, bash, and R to detect viral genomes in Staphylococcus aureus genomes
· Compile a list of genes from the identified viral genomes
· Developing a feature to the PhageNet pipeline to find the probability of a viral gene conferring beneficial traits to the host bacterium

Teaching Assistant for Natural Sciences August 2016 - Present
Math015

· Led class assignments and discussions that introduce students to statistics and R
· Created labs that are approachable and encourages excellent coding practices

SIAM Applied Math Challenge - UC Merced March 2021
Team Lead

· Mentored a group of 4 students in the development of a SIR model in Python
· Conducted a sensitivity analysis on parameters of interest
· Received second place in model solution and presentation

Lawrence Livermore National Lab Summer 2019
Team lead for the LLNL Data Science challenge

· Led a team of 5 students in the development of a machine learning algorithm, in Python, to improve the antibody binding affinities
· Improved model's predictive performance by identifying the most critical features in our data set

Department of Energy - Joint Genome Institute July 2017 - August 2017
Genomic Bioinformatician Intern

· Developed software to identify chimera sequences generated by the Oxford Nanopore MinION
· Reviewed code associated with the handling of data produced by the Oxford Nanopore MinION
· Learned industry standards necessary for collaborating with code scripts, data, and cluster usage

FUNDING SOURCES

NSF Research Traineeship - Intelligent Adaptive Systems
NIH Research Enhancement Award (R15)

ACADEMIC ACHIEVEMENTS

Accepted into NSF Research Traineeship - Intelligent Adaptive Systems (NRT) program
Completed the NSF-funded Interdisciplinary Computational Graduate Education Program (ICGE)
Deans list award in Brooklyn College Fall 2012, and Spring 2013

EXTRA-CURRICULAR

Academics Affairs Officer in the Graduate Student Association - 2019
Quantitative and Systems Biology - Recruitment chair - 2017

Active member of BiotaQ. An outreach program designed to demystify STEMC-majors

Founding member of the graduate student group Data Science at UC Merced - 2017

CONFERENCES & PRESENTATIONS

August 2022 - Selected as a top presenter in the summer slam event at LLNL; Invited to present for the Livermore Lab Foundation.

April 2021 - Poster presentation at the Quantitative and Systems Pharmacology. Received 3rd place.

January 2020 - Poster presentation at the Mid Winter Conference of Immunologists

November 2019 - Poster presentation at the Quantitative and Systems Pharmacology

WORKSHOPS

March 2018 - Mentor for the UC Merced Research Vix Workshop

June 2018 - Mentor for the Python workshop at UC Merced

Abstract

Mathematical modeling of IL-2 dysregulation
in the pathogenesis of autoimmune disease

Doctor in Philosophy

in

Quantitative and Systems Biology

by

Jonathan Michael Anzules

University of California, Merced

2022

Chair of Advisory Committee: Professor Justin Yeakel

Autoimmune disease is driven by the dysregulation of one's own immune system and its inability to distinguish self from foreign; however, the etiology of autoimmunity is not wholly understood. I have developed a data-driven mathematical model which quantifies the dysregulation of autoimmune disease pathogenesis. The model explores the dynamics of homeostatic expansion during early immune development in healthy BALB/c mice (Wildtype; WT) and the pathogenesis of autoimmune disease in an interleukin-2 (IL-2) deficient BALB/c mouse model (IL-2 KO). This study focuses on the interactions between naive CD4 T cells, regulatory CD4 T cells (Tregs), activated CD4 T cells, and the dynamic influence of IL-2 on Treg functionality and survival. Removal of the IL-2 cytokine creates a homeostatic imbalance that leads to the rapid onset of autoimmune disease. Modeling allows us to predict the behavior of immune cells, quantify the suppressive differences between a healthy and an autoimmune system, and explore the parameters that can prevent autoimmune disease. Currently, no published models have quantitatively studied this specific timeframe in combination with the immunological dynamics that prevent autoimmune disease.

CHAPTER ONE

Introduction: Autoimmune disease, mathematical modeling, and current progress in the field

1.1 Autoimmune disease

Autoimmune diseases (AD), such as systemic lupus, colitis, and autoimmune hemolytic anemia (AIHA), affect 80 to 120 million people in the United States [1]. These diseases are often life-threatening, difficult to diagnose, and incurable. Risk factors such as exposure to environmental irritants [3], family history of autoimmune disease [4], age, sex, and ethnicity [5] are known to increase the chances of developing autoimmune disease. However, despite our understanding of risk factors, we still do not fully understand the pathogenesis of AD and their prevalence is on the rise [2].

To understand autoimmune pathology, we must first understand the mechanism that prevents the immune system from recognizing self-antigens. Tolerance prevents the immune system from recognizing an antigen, specifically for the deterrence of AD; it prevents self-antigen recognition. In addition, regulatory T cells (Tregs) are crucial for maintaining immunological tolerance to self-antigens and preventing excessive immune responses detrimental to the host [91].

Although there are several treatment options for AD [92-94], these diseases are incurable, making it essential to recognize regulatory dysregulation before developing autoimmunity. Using mathematical modeling, I attempt to investigate the anomalies that develop in the Treg population before the failure of the immunological self-tolerance, with the understanding that this failure leads to the recognition of self-antigens and the development of autoimmune disease. I collected the data from healthy (wild type; WT) and autoimmune mouse model systems (IL-2 knockout; KO). In the KO mouse model, Treg functionality is disrupted, resulting in the rapid onset of autoimmunity [45, 51,52]. By creating a mathematical model that mimics the data of healthy and autoimmune systems, we may understand early dysregulation and forecast prevention strategies for AD.

Size, homeostasis, expansion, and function of Tregs are determined by IL-2 cytokine. As shown by the IL-2 KO mice model and system lupus erythematosus patients, IL-2 cytokine dysfunction may lead to the development of autoimmune illness [45, 51, 52, 95]. However, due to the short half-life of IL-2 (30 minutes) [95-98], it is challenging to experimentally study their effects on the immune system, particularly its maintenance of self-tolerance through Tregs. Using our mathematical model, we can investigate the dynamics of IL-2 and Tregs in self-tolerance and uncover dysregulation before the start of AD.

Two types of mathematical models can be formulated: qualitative and quantitative. The qualitative model does not implement any data for its calibration, and the quantitative does. I have developed a quantitative mathematical model, calibrated by in-house data, that can detect

early signs of dysregulation in the Treg growth trajectory and identify preventative measures for autoimmune disease.

Tolerance

To prevent and treat autoimmunity, we must understand the tolerance mechanism. Self-tolerance is the ability of the immune system to avoid activating against self-antigens. After tolerance develops, these antigens deactivate or eliminate lymphocytes that identify them. Tolerance to self-peptides is a crucial feature of the immune system; failure of this feature results in autoimmune disease development [22].

There are two mechanisms of tolerance: central and peripheral tolerance. For central tolerance, immature T cells are tested against self-peptides in the thymus. If immature T cell has a strong interaction with a self-peptide via its lymphocytes' T cell receptor (TCR), they are removed by apoptosis (negative selection). On the other hand, immature lymphocytes that recognize a self-peptide with low avidity survive this process and egress into the periphery (positive selection) as naïve T cells.

Central tolerance does not work perfectly, and some self-reactive cells still make their way to the periphery [21] where peripheral tolerance protects the body from AD development. Survival of naive T cells in the periphery depends on signaling provided by antigen-presenting cells (APC). Naive T lymphocytes are supplied with the survival signal when the TCR has a low-affinity interaction with self-peptides. Conversely, a strong interaction can lead to the deletion of that specific clonotype or become anergic [22]. Additionally, the equilibrium between Tregs and activated T cells maintains peripheral self-tolerance and immunological homeostasis. In many ways, Tregs inhibit the activation and proliferation of other cells and contribute to the maintenance of self-tolerance [99].

Amongst math-oriented immunologists, it is theorized that competition for survival signals creates an environment that exerts selective pressure on a highly diverse repertoire of naive T cell clonotypes [23-25]. T cell diversity, an essential feature of the immune system, maximizes the potential of recognizing any pathogen that invades the body [26]. This competition for survival signals creates a niche environment for the survival of a specific set of naive T cell clonotypes. The accessibility to interact with self-peptides, presented by APCs, sets the size limit of a niche population of naive T cells. Mandl *et al.* postulates that over time, as the immune system accumulates the number of pathogens it encounters, T cell receptors with a more robust interaction with self-peptides dominate the naive T cell repertoire. They found evidence that TCRs that bind well to foreign antigens also bind well to self-antigens. This skews the system towards a more efficient recognition of pathogens that can potentially pose a danger to the host in the form of autoimmune disease [26]. The results from Mandl et al. may explain why autoimmune disease becomes more prevalent as the population ages [100].

The story of tolerance becomes more complicated when we consider that Tregs depend on survival signals produced by activated T cells in the form of IL-2 cytokine (more on this ahead). A mathematical model developed by Carneiro *et al.* studies the theoretical dynamics of repertoire selection. They conclude that a subset of autoreactive effector and Treg cells regulate each other's growth [27], suggesting that a low-grade amount of self-activation is necessary to maintain a basal population of Tregs.

Regulatory T cells

In 1995, Sakaguchi et al. identified a population of CD4+CD25+ T cells in mice that accounted for 5-10% of all CD4 T cells. In vitro and in vivo, these CD4+CD25+ T cells demonstrated powerful regulatory activities [101]. The thymus is the source of naturally generated CD4+CD25+ T cells since thymectomy on day 3 of life results in negligible to undetectable peripheral CD4+CD25+ T cells in BALB/c mice [111]. From naïve T cells, induced regulatory T cells are produced de novo extrathymically.

In 2000, Chatila et al. identified mutations in the gene encoding the transcription factor forkhead box P3 (Foxp3), previously named JM2, as the cause of X-linked autoimmunity-allergic dysregulation syndrome, causing an autoimmune lymphoproliferation disorder [102]. In addition, seminal investigations showed that Foxp3 controls Treg cell activity in scurfy mice, which develop a lymphoproliferative illness due to Treg functional deficiency [103, 104]. Therefore, I used foxp3 as a cellular marker for regulatory CD4 T cells in this project.

Regulation of the immune reaction requires a balance between mounting a protective immune response and preventing a harmful inflammatory response. Tregs prevents an out-of-control immune response that can cause tissue damage, exposing more self-antigens and potentially instigating an even more robust immune response to self-antigens. There is significant evidence of dysregulation in the Treg population that can lead to autoimmune disease. Understanding the systemic influence of Tregs is critical and serves as the primary motivator for developing a mathematical model.

Dysregulation of Tregs can be seen in the autoimmune disease systemic lupus erythematosus (SLE), where the immune system attacks widespread tissue. Tissues targeted in this disease include joints, skin, brain, lungs, kidneys, and blood vessels. Tregs are significantly decreased in patients with active SLE compared to control and inactive SLE groups [12]. Another systemic disease, autoimmune hemolytic anemia (AIHA) is an autoimmune disease where the immune system creates autoantibodies that target red blood cells (RBC) for destruction. One study found that patients with AIHA had 4.63% Tregs circulating in their blood, while the control group had 9.76% [13]. Mgadmi et al. used repeated rat RBC immunization into C57BL/6 to study the immune response against RBC. Treatment with anti-CD25 depletes the Treg population. In this study, treatment with anti-CD25 before immunization with rat RBCs increased the incidence of AIHA from 30% to 90% [14].

Tregs prevent autoimmune disease

In addition to the dysregulation seen of the Treg population in AD, there is evidence that Tregs may inhibit and prevent autoimmune illness. For example, colitis is an organ-specific inflammatory disease affecting the colon's inner lining. This disease is characterized by chronic inflammation that can lead to losing blood supply to the area, infection, and inflammatory bowel disease. Scientists discovered that CD4+ Tregs could inhibit colitis. This opened a new focus on signaling pathways that can give an avenue of therapeutic influence, such as manipulating Treg function via CTLA-4 and TGF-$\boldsymbol{\beta}$ [15-17].

Type 1 diabetes (T1D) is one example of an organ-specific disease where Treg defects are observed [18]. Our knowledge of autoimmune diseases has accumulated enough to allow disease prevention and treatment attempts. In nonobese diabetic (NOD) mice, Grinberg-Bleyer et al., reversed T1D by the injection of low-dose IL-2 cytokine [19]. The infusion of IL-2 expands the survivability of Tregs and enhances their ability to prevent AD.

Bluestone, et al. developed a path for the therapeutic care of T1D in patients. The treatment involves the isolation and in vitro expansion of patient Tregs, then reinfusion of expanded Tregs back into the patients. This experiment is in a phase 1 clinical trial [20], where they primarily test for the safety of this procedure on people. They report that the infusion of Tregs has been well tolerated, with no additional concerns for safety. These are promising results for future therapeutic strategies for autoimmune disease.

Peripheral tolerance and Treg suppression

How do Tregs suppress and maintain peripheral tolerance? Tregs exercise their suppressive function in a contact-dependent and contact-independent manner. These include cytotoxic mechanisms, inhibitory cytokines, suppression of APCs, and the disruption of metabolic pathways.

Cytolysis, via the secretion of granzymes, is a strength of Natural Killer (NK) cells and CD8 cytotoxic T lymphocytes (CTL). CD4+Foxp3+ Tregs also possess cytotoxic properties by the differential expression of granzymes B, and perforin [28-30, 105-110]. However, this function can potentially prove to be problematic: It has been shown that Tregs can hamper the removal of cancer cells by eliminating NK and CTLs via granzyme B and perforin [31]. Although Treg suppression is essential for the maintenance of tolerance and immune suppression, their overperformance can be problematic for the host.

In addition to Tregs directly affecting T effector cells, they can also modulate the function and the maturation of dendritic cells (DC). DCs are types of antigen-presenting cells whose primary function is to process antigenic material and present it on the surface for T cells to interact and identify. Direct interactions between Tregs and DCs attenuate effector T cell activation [32, 33]. This process involves the co-stimulatory molecule CTLA4, which Tregs constitutively express. In addition, Tregs can induce the expression of indoleamine 2,3-dioxygenase in DCs. This potent regulatory molecule causes the production of pro-apoptotic metabolites, resulting in the suppression of activated T cells [34]. Tregs can downregulate the expression of co-stimulatory molecules [35], suppressing the activation of naive T cells. Lastly, several studies have demonstrated that Tregs influence the maturation and function of DCs [36-40].

The influence of Tregs on the metabolic function of effector T cells is still unclear but worthy of mention as a mechanism of Treg suppression. Tregs constitutively express CD25, which allows for their identification by the high levels of CD25 expression on their cellular surface. CD25 is a high-affinity receptor for the IL-2 cytokine. Activated effector T cells require IL-2 for the initial stages of activation and survival. In one study, Duhoit *et al.* suggest that Tregs can induce cytokine-deprivation-mediated apoptosis [41]. Lastly, the co-expression of CD39 and CD73 on Tregs may trigger a signaling cascade in effector T cells that downregulate their function [42, 43].

As a community, we understand the components involved in regulating tolerance and some mechanisms of Treg suppression, but how these mechanisms prevent the development of AD is still an active field of investigation. There are, however, theories of how the Treg function creates a threshold that must be overcome by a specific clonotype of naive T cells to trigger an immune response [44]. The process of central tolerance, selecting naive T cells with a low-level affinity for self-antigens, the competitive environment for naive T cells, and the relentless suppression by Tregs create an environment where self-reactive cells are unlikely to trigger an immune response.

If we theorize that Tregs establishes a ‘threshold’ for activation, we can then assume that there must be a concentration of Tregs to maintain this threshold. This concentration must be enough to counteract the low-grade immune response to self-antigens while also not preventing an immune response to a pathogen. This balance between T cells and Tregs is well understood as a requirement for proper immune function. In a normal and healthy system, it is expected for Tregs to represent ~5-15% of the entire T cell population [45-48]. However, how this balance is maintained is still unclear. The study of autoimmune disease development has moved past patient data towards a more sophisticated and systemic approach using mouse autoimmune models.

1.2 IL-2 deficient mouse model system

Several inbred mouse models have been developed to study the dynamics of autoimmune disease. Because of the complex nature of autoimmune disease and the uncertainty around its pathogenesis, mouse models offer us a manipulatable way to study AD dynamics. However, these systems are not perfect and sometimes eliminate a critical feature required for immune homeostasis. Eliminating these vital features leads to the rapid onset of AD, which can potentially mask the subtle differences that must occur for the development of autoimmune disease. Despite this, mouse models still provide a great deal of insight into the dynamics of AD and have provided insight into the therapeutic avenues of autoimmune diseases like T1D, lupus, and rheumatoid arthritis.

Many murine models have been developed to study the dynamics of autoimmune disease, and they fall under three categories; induced, spontaneous, and genetically engineered. A small sample of the possible mice models that exist include: NOD mice that spontaneously develop a form of T1D [49]; Collagen-induced arthritis in DBA/1 mice [50]; and IL-2 knockout (IL-2 KO) mice that can develop systemic lupus erythematosus, Crohn’s disease and AIHA [45, 51, 52]. Treg function is impaired in the IL-2 KO mouse model. For this project, however, I will use the IL-2 KO mouse model to investigate Tregs' role in self-tolerance mathematically.

IL-2 Cytokine

Historically the IL-2 cytokine was named T cell growth factor because of its ability to stimulate proliferative growth in T cells [53]. IL-2 is mainly expressed by activated CD4 T cells in response to antigen stimulation but can also be produced by CD8 T cells and various other immune cells [54]. IL-2 promotes CD4 T cells, CD8 T cells, and NK cells, proliferation and induces cytolytic activity in CD8 T cells [55]. When the IL-2-deficient mouse was generated, the story expanded.

As Katzman et al. [56] point out, there are opposing functions to the IL-2 cytokine. IL-2 binds to a complex of receptors to induce intracellular signaling. This complex includes the IL-2Rα (CD25), IL-2Rβ (CD122), and the common gamma (γc) chain (CD132). Defects in any of these receptor components result in severe autoimmunity [57]. For example, in the IL-2 KO mouse model, where IL-2 is depleted, all mice die between 18-36 days on the BALB/C genetic background from a combination of autoimmune hemolytic anemia and bone marrow failure [58].

IL-2 and Tregs

Treg size, homeostasis, and expansion are dependent on the availability of IL-2. Survival and function are also reliant on the presence of IL-2 for activated Tregs. In experiments where IL-2 is either removed or the receptor blocked with anti-CD25, significant depletion in Treg population size and function is observed, resulting in the progression of AD [59].

In addition to IL-2 supporting the population size of Tregs, it also plays a role in their suppressive abilities. When Tregs are pre-treated with IL-2 there is a marked increase in their suppressive abilities in co-culture assays with effector CD4 T cells [60]. Since Treg survivability depends on IL-2, Barron et al. artificially extended the life of Tregs in IL-2 KO mice by eliminating the pro-apoptotic BH3-only protein, Bim. In these experiments, Treg survival increased, but lethal levels of autoimmunity still occurred, because IL-2 plays a critical role in the suppressive function of Tregs [61].

The IL-2 KO system has several advantages for studying the progression of autoimmune disease: disease is rapid, the major underlying tolerance defect is known (Treg deficiency and reduced Treg suppressive function), and disease can be manipulated by eliminating various signals (CD28, CD40, dendritic cell help) [62]. Early signs of autoimmune disease have been observed by day 12 of development [51, 63] in IL-2 KO mice. Lethal autoimmunity is observed by day 19 on the BALB/c genetic background. This allows us to track the deviation from a healthy developmental trajectory to an autoimmune state. In combination with modern high throughput data collection and mathematical modeling, we have the potential to simulate the instability that occurs globally in a system to study the development of autoimmune disease and identify critical characteristics of immune imbalance before the onset of autoimmune disease.

1.3 A systems biology approach

The immune system is diverse, containing a heterogeneous mix of cell types in unique states of differentiation and activation. Moreover, the diversity in cell state, location, and molecular organization or immune cells vary within and across the same organism. For the most part, immunology research has focused on specific cellular and molecular cell components by using powerful animal and in vitro models [64]. However, how these populations interact, influence each other, and function as a complete system has not been investigated robustly [65]. In part, this is a consequence of many relevant parameters (number and location of specific cell times) and mechanistic complexities (gene expression dynamics, circulating cytokines, and growth factors).

Fortunately, modern advances in data acquisition – including the development of multiplexed high-throughput technologies like proteomic and transcriptomic profiling [66, 67], single-cell technologies [68], DNA sequencing [69], and multicolor flow cytometry [70] – have provided greater resolution into the temporal dynamics of immune systems. This allows the opportunity to develop, validate and study system-wide-level mathematical models of immunological phenomena. In addition, these higher-resolution data offer the hope for advanced and personalized therapeutics for human diseases, including autoimmune diseases. However, these realizations will only be realized if underlying immune system dynamics can be mechanistically predicted with mathematical models which will inform these personalized therapies [71]. Developing and validating mathematical models requires an interdisciplinary approach to integrate biological and physiological knowledge, chemical and physical properties as well as clinical and omics data.

1.4 Immune mathematical modeling

The reductionist approach of immunology allowed for the discovery of fundamental features of the immune system ranging from discriminating between self- and non-self-antigens to the persistent suppressive ability of Tregs. From these features, we can begin to organize a conceptual model of autoimmune disease onset from IL-2 depletion.

Mathematical modeling can become a powerful tool for knowledge discovery as it combines all known features into a single cohesive model. More specifically, a mathematical model serves many important roles such as: explaining existing observations, aiding in the generation of new hypotheses, understanding the impact of assumptions made in the model, generating *in silico* data in comparison to experimental data [72], improving the organization of data generated from experiments [73], offering search criteria for ideas that can be tested experimentally (reducing the time and cost of exploring with large experiments), discovering the underlying mechanisms driving certain phenomena [74], exploring the feasibility of an intuitive argument, and making theoretical contributions to the understanding of immunological systems [75].

Comparisons between mathematical models and biological systems can follow two approaches: qualitative and quantitative models. In both, a mathematical formulation of a biological system is put together, often as an ordinary differential equation (ODE) representing the time-varying dynamics. However, once the structure of these models is complete, different approaches can be taken to explore the phenomenon in greater detail. For qualitative models, the main motivator is to explore the dynamics of the model without explicitly matching its quantitative output to experimental observation. For example, the mathematical model can be probed to determine conditions necessary for stability/instability [76], the probability that certain behavior occurs [77], or to investigate parameters that cause the bifurcation of the system into distinct behavioral patterns [78]. In quantitative comparisons, mathematical models are precisely developed in conjunction with and calibrated by experimental data [79] or use kinetic rates to try and predict the behavior of biochemical pathways in autoimmune disease [80]. Far from disjoint categories, there can be a combination of both qualitative and quantitative analysis of the same system of differential equations [81].

1.5 Qualitative modeling and autoimmune diseases

Borghans et al. proposed one of the first mathematical models of immune system development including Tregs and autoimmune dynamics [82]. They aimed to determine the circumstances required to avoid autoimmune illness using "T cell vaccination," in which the immune system is prepared to prevent autoimmune disease through the injection of auto-reactive T cells. Although they note their model “is based on detailed data on experimental autoimmune encephalomyelitis”, the authors did not explicitly indicate how data was used to calibrate their mathematical model. Intriguingly, their model predicted qualitative differences to varying dose size of autoreactive T cells when inoculated.

More recently, mathematical models that involve autoimmunity and the dynamics of Tregs have become increasingly complex. Models have begun to introduce differentiation from an active to an inactive state of CD4 T cells [44], the developmental process from somatic cells to active Tregs and T cells [83], and IL-2 dependent replication [84]. These studies aimed to identify conditions of the immune system which make it possible to perturb autoimmune disease by studying the qualitative results of their models. Again, these models were not fine-tuned to data, but focused on the phenomenological behavior possible from the models and used past data as a qualitative guide in development. As such, their theoretical probing of autoimmune dysregulation

could guide the development of experimental conditions necessary to answer these questions, but the models themselves did not lead to groundbreaking discoveries [84].

1.6 Quantitative modeling and autoimmune diseases

Quantitative comparisons between mathematical models and empirical data are far less common than qualitative ones. Moreover, it is even more rare to see quantitative comparisons when examining models focused on immune system dysregulation. Busse et al. developed the first quantitative model focused on Treg, effector T cells, and IL-2 cytokine dynamics, but not autoimmunity [85]. Although Tregs and IL-2 cytokine dynamics are intimately associated with homeostasis and the prevention of autoimmune disease, Busse et al., do not explore the dysregulation that may occur for an autoimmune disease to develop. Instead, they study temporal dynamics between IL-2 production, Treg, and effector cell consumption of IL-2, and the resulting proliferation of Treg and effector cells. They quantitatively identified the simulation threshold by IL-2 cytokine that led to different proliferative states. Their model was validated by fitting the model to in-house collected data.

Another important study in this field is the mathematical model developed by Garcia-Martinez et al. [87] of the IL-2 dynamics between Tregs and effector cells. Although the primary work in this study was qualitative, the mathematical model uses experimentally determined quantities and kinetic values (i.e., peripheral lymph nodes contain about 10^7 lymphocytes, 700-1000 IL-2 receptors per activated T cells, IL-2 internalization, and half-life rates). Garcia-Martinez et al, found how the system's steady-state could tend towards autoimmune disease when the autoreactive T cells outcompete the suppressive abilities of Tregs. Using experimentally determined rates is a useful strategy to predict the effects of drug therapies in the field of physiological based pharmacokinetic modeling and simulation (PBPK) [71]. However, this approach is problematic as values may vary between laboratories, and very few measure and estimate kinetic parameters [88, 89]. Due the heterogeneity of biological systems, temporal changes in machine behavior, and varying levels of technical skills can make interpreting kinetic rates within one's own lab difficult so, the over-reliance on precisely knowing kinetic rates pose challenges to precise quantitative calibration and predictions from mathematical models.

A recent study by Wong et al. used a combination of new imaging and computation approaches to study the dynamics between autoreactive T cells and Tregs at physiological numbers *in situ* [90]. In this study, they note that T cells that react to self-antigens transiently expand, produce IL-2 cytokine and then the progeny readily dies off, they are 'pruned' by Treg suppression. Using a combination of data analysis, machine learning, and mathematical modeling they identified parameter combinations that allow autoreactive T cells to subvert the control of Tregs and escape the pruning event. This work provides a strong example of an autoimmune study that collected data and calibrated a mathematical model with the data collected. This type of approach to mathematical modeling ensures that the immune field receives a model that is both useful and quantitatively accurate in its reflection of the phenomenon of interest.

1.7 Summary

The project defined in the following chapters involves the creation of a quantitative model of immune system development calibrated by experimental data. I used this model to study dynamics rarely seen in immunological quantitative models: Treg and effector T cell dynamics, IL-2 influence on Treg survival and functionality, and homeostatic expansion in neonatal mice.

Currently, there are no published models that quantitatively study this specific timeframe in combination with the immunological dynamics that prevent autoimmune disease.

References

1. American Autoimmune Related Diseases Association. (2011). The cost burden of autoimmune disease: the latest front in the war on healthcare spending. *American Autoimmune Related Diseases Association, Eastpointe, Michigan, USA*.
2. Dinse, Gregg E., et al. "Increasing prevalence of antinuclear antibodies in the United States." *Arthritis & Rheumatology* 72.6 (2020): 1026-1035.
3. Smyk, Daniel, et al. "Autoimmunity and environment: am I at risk?." Clinical reviews in allergy & immunology 42.2 (2012): 199-212.
4. Rai, Ekta, and Edward K. Wakeland. "Genetic predisposition to autoimmunity–what have we learned?." Seminars in immunology. Vol. 23. No. 2. Academic Press, 2011.
5. Lee, Briton, et al. "Race/ethnicity is an independent risk factor for autoimmune hepatitis among the San Francisco underserved." Autoimmunity 51.5 (2018): 258-264.
6. Shevach EM. Regulatory T cells in Baker PJ, Stashak PW, Amsbaugh DF, Kronenberg M, et al. RNA transcripts for autoimmmunity. Prescott B. Regulation of the antibody I-J polypeptides are apparently not encoded Annu Rev Immunol 2000;18:423–449.
7. Sakaguchi S. Regulatory T cells: key murine major histocompatibility complex. controllers of immunologic self-tolerance. thymic-derived suppressor cells. Proc Natl Acad Sci USA Cell 2000;101:455–458.
8. Mason D, Powrie F. Control of immune Okumura K, Tada T. Regulation of Webb DR, Semenuk G, Krupen K, Jendrisak pathology by regulatory T cells. homocytotropic antibody formation in the GS, Bellone CJ. Purification and analysis of Curr Opin Immunol 1998;10:649–655.
9. Bach JF, Chatenoud L. Tolerance to islet a T cell hybridoma specific for autoantigens and type I diabetes. J Immunol 1971;107:1682–1689. phenyltrimethylamino hapten. Annu Rev Immunol 2001;19:131–161
10. Salomon B, Bluestone JA. Complexities of 21. Mosmann TR, Coffman RL. TH1 and TH2 CD28/B7: CTLA-4 costimulatory pathways J Exp Med 1981;153:1533–1546. cells: different patterns of lymphokine in autoimmunity and transplantation. 14. Green DR, Gershon RK. Contrasuppression: secretion lead to different functional Annu Rev Immunol 2001;19:225–252
11. Chatenoud, Lucienne, Benoît Salomon, and Jeffrey A. Bluestone. "Suppressor T cells–they're back and critical for regulation of autoimmunity!." Immunological reviews 182.1 (2001): 149-163.
12. Crispin, Jose C., Araceli Martınez, and Jorge Alcocer-Varela. "Quantification of regulatory T cells in patients with systemic lupus erythematosus." Journal of autoimmunity 21.3 (2003): 273-276.
13. Ahmad, E., T. Elgohary, and H. Ibrahim. "7 Naturally Occurring Regulatory T Cells and Interleukins 10 and 12 in the Pathogenesis of Idiopathic Warm Autoimmune Hemolytic Anemia." Journal of Investigational Allergology and Clinical Immunology 21.4 (2011): 297.
14. Mqadmi, Amina, Xiaoying Zheng, and Karina Yazdanbakhsh. "CD4+ CD25+ regulatory T cells control induction of autoimmune hemolytic anemia." Blood 105.9 (2005): 3746-3748.
15. Read, Simon, Vivianne Malmström, and Fiona Powrie. "Cytotoxic T lymphocyte–associated antigen 4 plays an essential role in the function of CD25+ CD4+ regulatory

cells that control intestinal inflammation." The Journal of experimental medicine 192.2 (2000): 295-302.

16. Liu, S. M., Sutherland, A. P., Zhang, Z., Rainbow, D. B., Quintana, F. J., Paterson, A. M., ... & Kuchroo, V. K. (2012). Overexpression of the Ctla-4 isoform lacking exons 2 and 3 causes autoimmunity. *The Journal of Immunology*, *188*(1), 155-162.
17. Joller, N., Lozano, E., Burkett, P. R., Patel, B., Xiao, S., Zhu, C., ... & Kuchroo, V. K. (2014). Treg cells expressing the coinhibitory molecule TIGIT selectively inhibit proinflammatory Th1 and Th17 cell responses. *Immunity*, *40*(4), 569-581.
18. Hull, Caroline M., Mark Peakman, and Timothy IM Tree. "Regulatory T cell dysfunction in type 1 diabetes: what's broken and how can we fix it?." Diabetologia 60.10 (2017): 1839-1850.
19. Grinberg-Bleyer, Yenkel, et al. "IL-2 reverses established type 1 diabetes in NOD mice by a local effect on pancreatic regulatory T cells." Journal of Experimental Medicine 207.9 (2010): 1871-1878.
20. Bluestone, Jeffrey A., et al. "Type 1 diabetes immunotherapy using polyclonal regulatory T cells." Science translational medicine 7.315 (2015): 315ra189-315ra189.
21. Parish, Ian A., and William R. Heath. "Too dangerous to ignore: self-tolerance and the control of ignorant autoreactive T cells." Immunology and cell biology 86.2 (2008): 146-152.
22. Abbas, Abul K., Andrew H. Lichtman, and Shiv Pillai. Cellular and molecular immunology E-book. Elsevier Health Sciences, 2014.
23. Stirk, Emily R., Carmen Molina-París, and Hugo A. van den Berg. "Stochastic niche structure and diversity maintenance in the T cell repertoire." Journal of theoretical biology 255.2 (2008): 237-249.
24. Desponds, Jonathan, et al. "Population dynamics of immune repertoires." Mathematical, computational and experimental T cell immunology. Springer, Cham, 2021. 203-221.
25. De Boer, Rob J., and Alan S. Perelson. "T cell repertoires and competitive exclusion." Journal of theoretical biology 169.4 (1994): 375-390.
26. Mandl, Judith N., et al. "T cell-positive selection uses self-ligand binding strength to optimize repertoire recognition of foreign antigens." Immunity 38.2 (2013): 263-274.
27. Carneiro, Jorge, et al. "When three is not a crowd: a crossregulation model of the dynamics and repertoire selection of regulatory CD4+ T cells." Immunological reviews 216.1 (2007): 48-68.
28. Grossman, W. J. et al. Differential expression of granzymes A and B in human cytotoxic lymphocyte subsets and T regulatory cells. Blood 104, 2840–2848 (2004).
29. McHugh, R. S. et al. CD4+ CD25+ immunoregulatory T cells: gene expression analysis reveals a functional role for the glucocorticoid-induced TNF receptor. Immunity 16, 311–323 (2002).
30. Gondek, D. C., Lu, L. F., Quezada, S. A., Sakaguchi, S. & Noelle, R. J. Cutting edge: contact-mediated suppression by CD4+ CD25+ regulatory cells involves a granzyme B-dependent, perforin-independent mechanism. J. Immunol. 174, 1783–1786 (2005).
31. Cao, X. et al. Granzyme B and perforin are important for regulatory T cell-mediated suppression of tumor clearance. Immunity 27, 635–646 (2007).
32. Tang, Q. et al. Visualizing regulatory T cell control of autoimmune responses in nonobese diabetic mice. Nature Immunol. 7, 83–92 (2006).
33. Tadokoro, C. E. et al. Regulatory T cells inhibit stable contacts between CD4+ T cells and dendritic cells in vivo. J. Exp. Med. 203, 505–511 (2006).

34. Fallarino, F. et al. Modulation of tryptophan catabolism by regulatory T cells. Nature Immunol. 4, 1206–1212 (2003).
35. Cederbom, L., Hall, H. & Ivars, F. CD4+ CD25+ regulatory T cells down-regulate co-stimulatory molecules on antigen-presenting cells. Eur. J. Immunol. 30, 1538–1543 (2000).
36. Serra, P. et al. CD40 ligation releases immature dendritic cells from the control of regulatory CD4+ CD25+ T cells. Immunity 19, 877–889 (2003).
37. Kryczek, I. et al. Cutting edge: induction of B7-H4 on APCs through IL-10: novel suppressive mode for regulatory T cells. J. Immunol. 177, 40–44 (2006).
38. Lewkowich, I. P. et al. CD4+ CD25+ T cells protect against experimentally induced asthma and alter pulmonary dendritic cell phenotype and function. J. Exp. Med. 202, 1549–1561 (2005).
39. Houot, R., Perrot, I., Garcia, E., Durand, I. & Lebecque, S. Human CD4+ CD25high regulatory T cells modulate myeloid but not plasmacytoid dendritic cells activation. J. Immunol. 176, 5293–5298 (2006).
40. Misra, N., Bayry, J., Lacroix-Desmazes, S., Kazatchkine, M. D. & Kaveri, S. V. Cutting edge: human CD4+ CD25+ T cells restrain the maturation and antigen-presenting function of dendritic cells. J. Immunol. 172, 4676–4680 (2004).
41. Duthoit, C. T., Mekala, D. J., Alli, R. S. & Geiger, T. L. Uncoupling of IL-2 signaling from cell cycle progression in naive CD4+ T cells by regulatory CD4+ CD25+ T lymphocytes. J. Immunol. 174, 155–163 (2005).
42. Deaglio, S. et al. Adenosine generation catalyzed by CD39 and CD73 expressed on regulatory T cells mediates immune suppression. J. Exp. Med. 204, 1257–1265 (2007).
43. Kobie, J. J., Shah, P. R., Yang, L., Rebhahn, J. A., Fowell, D. J., & Mosmann, T. R. (2006). T regulatory and primed uncommitted CD4 T cells express CD73, which suppresses effector CD4 T cells by converting 5′-adenosine monophosphate to adenosine. *The Journal of Immunology*, *177*(10), 6780-6786.
44. Khailaie, Sahamoddin, et al. "A mathematical model of immune activation with a unified self-nonself concept." Frontiers in immunology 4 (2013): 474.
45. Hoyer, Katrina K., et al. "Interleukin-2 in the development and control of inflammatory disease." Immunological reviews 226.1 (2008): 19-28.
46. Su, M. A., Stenerson, M., Liu, W., Putnam, A., Conte, F., Bluestone, J. A., & Anderson, M. S. (2009). The role of X-linked FOXP3 in the autoimmune susceptibility of Turner Syndrome patients. Clinical immunology, 131(1), 139-144.
47. Larmonier, Nicolas, et al. "Tumor-derived CD4+ CD25+ regulatory T cell suppression of dendritic cell function involves TGF-β and IL-10." Cancer Immunology, Immunotherapy 56.1 (2007): 48-59.
48. Zhao, L., Sun, L., Wang, H., Ma, H., Liu, G., & Zhao, Y. (2007). Changes of CD4+ CD25+ Foxp3+ regulatory T cells in aged Balb/c mice. Journal of leukocyte biology, 81(6), 1386-1394.
49. Atkinson, Mark A., George S. Eisenbarth, and Aaron W. Michels. "Type 1 diabetes." The Lancet 383.9911 (2014): 69-82.
50. Joosten, L. A., Helsen, M. M., van de Loo, F. A., & van den Berg, W. B. (1996). Anticytokine treatment of established type II collagen–induced arthritis in DBA/1 mice: a comparative study using anti-TNFα, anti–IL-1α/β, and IL-1Ra. Arthritis & Rheumatism, 39(5), 797-809.
51. Sadlack, B., J. Lo¨hler, H. Schorle, G. Klebb, H. Haber, E. Sickel, R. J. Noelle, and I. Horak. 1995. Generalized autoimmune disease in interleukin-2-deficient mice is triggered

by an uncontrolled activation and proliferation of CD4+ T cells. Eur. J. Immunol. 25: 3053–3059
52. Morel, Laurence. "Mouse models of human autoimmune diseases: essential tools that require the proper controls." PLoS biology 2.8 (2004): e241.
53. Gillis, Steven, et al. "T cell growth factor: parameters of production and a quantitative microassay for activity." The Journal of Immunology 120.6 (1978): 2027-2032.
54. Kristensen NN, Christensen JP, Thomsen AR. High numbers of IL-2-producing CD8+ T cells during viral infection: correlation with stable memory development. J Gen Virol. 2002; 83:2123–2133. [PubMed: 12185265]
55. Watson J, Aarden LA, Shaw J, Paetkau V. Molecular and quantitative analysis of helper T cell replacing factors on the induction of antigen-sensitive B and T lymphocytes. J Immunol. 1979; 122:1633–1638. [PubMed: 109511]
56. Katzman, Shoshana D., et al. "Opposing functions of IL-2 and IL-7 in the regulation of immune responses." Cytokine 56.1 (2011): 116-121.
57. Aoki, Christopher A., et al. "IL-2 receptor alpha deficiency and features of primary biliary cirrhosis." Journal of autoimmunity 27.1 (2006): 50-53.
58. Gravano, D. M., Al-Kuhlani, M., Davini, D., Sanders, P. D., Manilay, J. O., & Hoyer, K. K. (2016). CD8+ T cells drive autoimmune hematopoietic stem cell dysfunction and bone marrow failure. *Journal of autoimmunity*, *75*, 58-67.Setoguchi R, Hori S, Takahashi T, Sakaguchi S. Homeostatic maintenance of natural Foxp3(+) CD25(+) CD4(+) regulatory T cells by interleukin (IL)-2 and induction of autoimmune disease byIL-2 neutralization. J Exp Med. 2005; 201:723–735. [PubMed: 15753206]
59. Tang, Qizhi, et al. "In vitro–expanded antigen-specific regulatory T cells suppress autoimmune diabetes." The Journal of experimental medicine 199.11 (2004): 1455-1465.
60. Barron L, Dooms H, Hoyer KK, Kuswanto W, Hofmann J, O'Gorman WE, Abbas AK. Cutting edge: mechanisms of IL-2-dependent maintenance of functional regulatory T cells. J Immunol. 2010; 185:6426–6430. [PubMed: 21037099]
61. Guiducci, Cristiana, et al. "CD40/CD40L interaction regulates CD4+ CD25+ T reg homeostasis through dendritic cell-produced IL-2." European journal of immunology 35.2 (2005): 557-567.
62. Mullins, Genevieve N., et al. "T cell signaling and Treg dysfunction correlate to disease kinetics in IL-2Rα-KO autoimmune mice." Scientific reports 10.1 (2020): 1-16.
63. Masopust, D., Sivula, C. P., & Jameson, S. C. (2017). Of mice, dirty mice, and men: using mice to understand human immunology. The Journal of Immunology, 199(2), 383-388.
64. Germain, Ronald N., and Pamela L. Schwartzberg. "The human condition: an immunological perspective." Nature immunology 12.5 (2011): 369-372.
65. Chaussabel, D. et al. (2010) Assessing the human immune system through blood transcriptomics. BMC Biol. 8, 84
66. Kingsmore, S.F. (2006) Multiplexed protein measurement: technologies and applications of protein and antibody arrays. Nat. Rev. Drug Discov. 5, 310–321
67. Shalek, A.K. et al. (2013) Single-cell transcriptomics reveals bimodality in expression and splicing in immune cells. Nature 498, 236–240
68. Shendure, J. and Aiden, E.L. (2012) The expanding scope of DNA sequencing. Nat. Biotechnol. 30, 1084–1094
69. Jahan-Tigh, Richard R., et al. "Flow cytometry." The Journal of investigative dermatology 132.10 (2012): e1.
70. Vizirianakis, Ioannis S., et al. "Tackling pharmacological response heterogeneity by PBPK modeling to advance precision medicine productivity of nanotechnology and

genomics therapeutics." Expert Review of Precision Medicine and Drug Development 4.3 (2019): 139-151.
71. Antia R, Ganusov V, Ahmed R (2005) The role of models in understanding CD8+ T-cell memory. Nat Rev Immunol 5:101–111
72. Shou W, Bergstrom C, Chakraborty A, Skinner F (2015) Theory, models and biology. eLIFE 4:e07,158
73. Seiden PE, Celada F (1992) A simulation of the humoral immune system. In: Perelson AS, Weisbuch G (eds) Theoretical and experimental insights into immunology. NATO ASI series, vol 66. pp 49–62
74. Caswell H (1988) Theory and models in ecology: a different perspective. Ecol Model 43:33–44
75. Numfor E, Bhattacharya S, Lenhart S, Martcheva M (2014) Optimal control in coupled within-host and between-host models. Math Model Nat Phenom 9(4):171–203
76. Figueroa-Morales N, León K, Mulet R (2012) Stochastic approximation to the T cell mediated specific response of the immune system. J Theor Biol 295:37–46
77. Fory´s U (2009) Stability and bifurcations for the chronic state in Marchuk's model of an immune system. J Math Anal Appl 352:922–942
78. Bains, Iren, et al. "Quantifying thymic export: combining models of naive T cell proliferation and TCR excision circle dynamics gives an explicit measure of thymic output." The Journal of Immunology 183.7 (2009): 4329-4336.
79. Gerstenberger, Brian S., et al. "Discovery of tyrosine kinase 2 (TYK2) inhibitor (PF-06826647) for the treatment of autoimmune diseases." Journal of Medicinal Chemistry 63.22 (2020): 13561-13577.
80. Leander R, Dai S, Schlesinger L, Friedman A (2012) A mathematical model of CR3/TLR2 crosstalk in the context of Francisella tularensis infection. PLoS Comput Biol 8(11):e1002,757
81. Borghans, José AM, et al. "T cell vaccination in experimental autoimmune encephalomyelitis: a mathematical model." The Journal of Immunology 161.3 (1998): 1087-1093.
82. Nicholson, Lindsay B., Konstantin B. Blyuss, and Farzad Fatehi. "Quantifying the role of stochasticity in the development of autoimmune disease." Cells 9.4 (2020): 860.
83. Alexander, H. K., and Lindi M. Wahl. "Self-tolerance and autoimmunity in a regulatory T cell model." Bulletin of mathematical biology 73.1 (2011): 33-71.
84. Grossman, Zvi. "Immunological paradigms, mechanisms, and models: Conceptual understanding is a prerequisite to effective modeling." Frontiers in immunology (2019): 2522.
85. Busse, Dorothea, et al. "Competing feedback loops shape IL-2 signaling between helper and regulatory T lymphocytes in cellular microenvironments." Proceedings of the National Academy of Sciences 107.7 (2010): 3058-3063.
86. García-Martínez, Karina, and Kalet León. "Modeling the role of IL-2 in the interplay between CD4+ helper and regulatory T cells: assessing general dynamical properties." Journal of theoretical biology 262.4 (2010): 720-732.
87. Boer RD, Perelson A (2013) Quantifying T lymphocyte turnover. J Theor Biol 327:45–87
88. Gadhamsetty S, Beltman J, de Boer R (2015) What do mathematical models tell us about killing rates during HIV-1 infection? Immunol Lett 168(1):1–6
89. Wong, Harikesh S., et al. "A local regulatory T cell feedback circuit maintains immune homeostasis by pruning self-activated T cells." Cell 184.15 (2021): 3981-3997.
90. Sakaguchi, Shimon. "Naturally arising CD4+ regulatory t cells for immunologic self-tolerance and negative control of immune responses." Annual review of immunology 22 (2004): 531.

91. Khan, H., Sureda, A., Belwal, T., Çetinkaya, S., Süntar, İ., Tejada, S., ... & Aschner, M. (2019). Polyphenols in the treatment of autoimmune diseases. *Autoimmunity reviews*, *18*(7), 647-657.
92. Jiang, J., Zhao, M., Chang, C., Wu, H., & Lu, Q. (2020). Type I interferons in the pathogenesis and treatment of autoimmune diseases. *Clinical Reviews in Allergy & Immunology*, *59*(2), 248-272.
93. Konforte, D., Diamandis, E. P., van Venrooij, W. J., Lories, R., & Ward, M. M. (2012). Autoimmune diseases: early diagnosis and new treatment strategies. *Clinical chemistry*, *58*(11), 1510-1514.
94. Lieberman, L. A., & Tsokos, G. C. (2010). The IL-2 defect in systemic lupus erythematosus disease has an expansive effect on host immunity. *Journal of Biomedicine and Biotechnology*, *2010*.
95. Malek, T. R., & Castro, I. (2010). Interleukin-2 receptor signaling: at the interface between tolerance and immunity. Immunity, 33(2), 153-165.
96. Lotze, M. T., Matory, Y. L., Ettinghausen, S. E., Rayner, A. A., Sharrow, S. O., Seipp, C. A., ... & Rosenberg, S. A. (1985). In vivo administration of purified human interleukin 2. II. Half life, immunologic effects, and expansion of peripheral lymphoid cells in vivo with recombinant IL 2. The Journal of Immunology, 135(4), 2865-2875.
97. Konrad, M. W., Hemstreet, G., Hersh, E. M., Mansell, P. W., Mertelsmann, R., Kolitz, J. E., & Bradley, E. C. (1990). Pharmacokinetics of recombinant interleukin 2 in humans. Cancer research, 50(7), 2009-2017
98. Schmidt, A., Oberle, N., & Krammer, P. H. (2012). Molecular mechanisms of treg-mediated T cell suppression. *Frontiers in immunology*, *3*, 51.
99. Vadasz, Z., Haj, T., Kessel, A., & Toubi, E. (2013). Age-related autoimmunity. BMC medicine, 11(1), 1-4.
100. Sakaguchi, S., Sakaguchi, N., Asano, M., Itoh, M., & Toda, M. (1995). Immunologic self-tolerance maintained by activated T cells expressing IL-2 receptor alpha-chains (CD25). Breakdown of a single mechanism of self-tolerance causes various autoimmune diseases. The Journal of Immunology, 155(3), 1151-1164.
101. Chatila TA, Blaeser F, Ho N, Lederman HM, Voulgaropoulos C,Helms C, et al. JM2, encoding a fork head-related protein, ismutated in X-linked autoimmunity-allergic disregulation syn-drome. J Clin Invest. 2000;106(12):R75–81
102. Fontenot JD, Gavin MA, Rudensky AY. Foxp3 programs the de-velopment and function of CD4+CD25+ regulatory T cells. NatImmunol. 2003;4(4):330–6.10.
103. Hori S, Nomura T, Sakaguchi S. Control of regulatory T cell de-velopment by the transcription factor Foxp3. Science.2003;299(5609):1057–61.
104. Grossman, W. J., Verbsky, J. W., Barchet, W., Colonna, M., Atkinson, J. P., & Ley, T. J. (2004). Human T regulatory cells can use the perforin pathway to cause autologous target cell death. *Immunity*, *21*(4), 589-601.
105. Gondek, D. C., Lu, L. F., Quezada, S. A., Sakaguchi, S., & Noelle, R. J. (2005). Cutting edge: contact-mediated suppression by CD4+ CD25+ regulatory cells involves a granzyme B-dependent, perforin-independent mechanism. *The journal of immunology*, *174*(4), 1783-1786.
106. Gondek, D. C., Lu, L. F., Quezada, S. A., Sakaguchi, S., & Noelle, R. J. (2005). Cutting edge: contact-mediated suppression by CD4+ CD25+ regulatory cells involves a granzyme B-dependent, perforin-independent mechanism. *The journal of immunology*, *174*(4), 1783-1786.
107. Lindqvist, C. A., Christiansson, L. H., Thörn, I., Mangsbo, S., Paul-Wetterberg, G., Sundström, C., ... & Loskog, A. S. (2011). Both CD4+ FoxP3+ and CD4+ FoxP3− T cells from patients with B-cell malignancy express cytolytic markers and kill autologous leukaemic B cells in vitro. *Immunology*, *133*(3), 296-306.
108. MacHugh, R. S., Piccirilo, C., Young, D., Shevach, E., Collins, M., & Byrne, C. (2002). CD4CD25 immunoregulatory T cells: gene expression analysis reveals a functional role for the glucocorticoid-induced TNF receptor. *Immunity*, *16*, 311-323.
109. Grossman, W. J., Verbsky, J. W., Tollefsen, B. L., Kemper, C., Atkinson, J. P., & Ley, T. J. (2004). Differential expression of granzymes A and B in human cytotoxic lymphocyte subsets and T regulatory cells. *Blood*, *104*(9), 2840-2848.

110. Asano, M., Toda, M., Sakaguchi, N., & Sakaguchi, S. (1996). Autoimmune disease as a consequence of developmental abnormality of a T cell subpopulation. The Journal of experimental medicine, 184(2), 387-396.

Chapter 2

Methods and results: Characterization of autoimmune disease and data preparation for mathematical modeling

To begin the characterization of autoimmune disease etiology, I must identify and isolate the relevant cellular populations. I will explain the logic for the collection days, the collection of cell populations, the experimental approach, and then explain the results from the data collected.

2.1 Experimental conditions

Days of data collection

There are a few known key timepoints that contribute to the development of autoimmune disease pathology in IL-2 KO BALB/c mice. I chose the timepoints of data collection described below to survey important days of disease development. I collected data from both WT and KO mouse models for each timepoint, day 56 when IL-2 KO mice are no longer alive (n = 3-4). (**Fig. 1**) outlines autoimmune developmental events of IL-2 KO mice and time points of data collection (green diamonds), followed by a list of the rationale behind the days chosen:

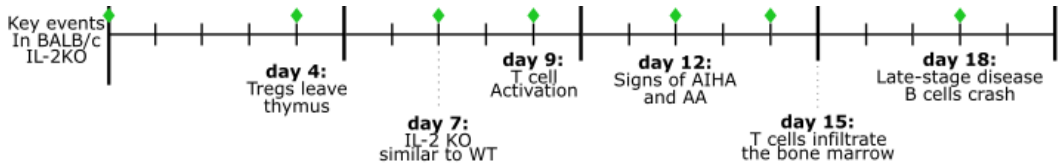

Figure 1. Timeline for data collection and autoimmune events. Days of IL-2 KO autoimmune events and days selected for data extraction (green diamonds). Each tick mark represents a day, and the larger ticks represent every 5 days.

- **Day 0:** Birth
- **Day 4**: Since thymectomy on day 3 of life results in negligible to undetectable peripheral CD4+CD25+ T cells in BALB/c mice, I assume that by day 4 Tregs ontogenetically begin to appear in the periphery from the thymus [1].
- **Day 7**: KO mice have an indistinguishable immune system compared to the WT [2].
- **Day 9**: Increased activation first observed in KO spleen [2].
- **Day 10:** Abnormal germinal center structures in KO mice observed [2].
- **Day 12**: Antibodies attached to red blood cells eventually causing autoimmune hemolytic anemia and aplastic anemia [3]; early bone marrow defects observed [4]
- **Day 16**: CD8 T cells infiltrate the bone marrow and proliferate [4]. These are mid-stage disease developments of autoimmune diseases; I am interested in the cellular changes before serious symptoms of autoimmune disease become life threatening.

- **Day 18+**: Late-stage aplastic anemia (AA) and AIHA; B cell population crashes [2]
- **Day 56**: Considered an adult mouse, only WT data was collected; IL-2 KO mice do not survive to this time point

Cell populations

At the beginning of the investigation, I did not know the structure of the mathematical model I would develop, but I knew the focus would be on the adaptive branch of the immune system. Therefore, I decided to track the growth trajectory of the significant cell populations in the adaptive immune system: CD4, CD8, B cells, and Tregs. Numerous studies show these populations are responsible for advancing and maintaining autoimmune disease in IL-2 KO [2, 5-7]

2.2 Data collection

Mouse husbandry

BALB/c IL-2-deficient mice were bred in our animal facility. BALB/c wild-type (WT) and IL-2 heterozygous littermates were used interchangeably as controls in all experiments as no hemizygosity effect is observed. Male and female mice were used in all experiments. Mice were euthanized by CO_2 asphyxiation followed by cervical dislocation or terminal bleed. All mice were bred and maintained in our specific pathogen-free facility in accordance with the guidelines of the Department of Animal Research Services at UC Merced. The UC Merced Institutional Animal Care and Use Committee approved all animal procedures.

Organ processing and cell isolation

Spleen and thymus were extracted, weighed, and processed through a wire mesh to generate single-cell suspensions. red blood cell (RBC) was lysed in lysis buffer was added to the sample, inverted for 30 seconds, left idle for 30 seconds, and then washed with phosphate-buffered saline (PBS). Samples were centrifuged at 1200 RPM for 5 minutes, supernatant discarded, and pellet resuspended in PBS. Cell counts were performed on a hemocytometer cell counter and resuspended to the desired concentration of cells.

Spleen and thymic cells were surface stained in PBS / 2% fetal-bovine-serum with fluorochrome-conjugated antibodies from **Table 1** for 30 minutes at 4°C in the dark. Cells were washed with PBS/2%FBS, centrifuged at 1200 RPM for 5 mins, supernatant discarded. Cells were then fixed with Foxp3/Transcription Factor Fixation/Permeabilization Kit (eBioscience) according to the manufacturer's instructions for intracellular proteins Ki67 and Foxp3.

Marker	Color	Concentration	Company	Clone	Purpose
TCR-**β**	FITC	1:400	Ebioscience	H57-597	Part of the T cell receptor complex for activation

CD4	PerCP-Cy5.5	1:1600	Ebioscience	RM4-5	Co-receptor for the T cell receptor complex in CD4 T cells
CD8	PE-eFluor 610	1:200	Biolegend	53-6.7	Co-receptor for the T cell receptor complex in CD8 T cells
CD19	PE-eFluor 610	1:800	Ebioscience	1D3	Important transmembrane protein in B cells that determines whether they live, proliferate, differentiate, or die
Foxp3	PE	1:100	Ebioscience	FJK-16s	Master regulator for the development and function of Tregs
Ki-67	PE Cy7	1:200	Ebioscience	SolA15	Nuclear protein associated with cellular proliferation
fixable viability dye	eFluor506	1:500	Ebioscience	-	Staining of live cells in order to differentiate between live and dead cells after fixation and permeabilization
CD69	APC-eFluor 780	1:50	Ebioscience	H1.2F3	Early T cell activation
CD62L	PE	1:1600	Biolegend	MEL-14	Cell adhesion molecule that allows cells to enter secondary lymphoid organs. Naive T cell marker
CD44	FITC	1:400	Biolegend	IM7	Cell-surface glycoprotein involved in lymphocyte activation

Table 1. Fluorescent staining panel. Staining panel used to identify the major cell populations and unique markers to further characterize these populations.

Cell Counting by hemocytometer

After RBC lysis, the remaining cells are diluted to a level where each quadrant in the hemocytometer contains 50-100 cells. After dilution, cells in each quadrant are counted and the average is determined using the following formula:

$$\textit{Total cell count} = \textit{Average cell count} \times \textit{Dilution Factor} \times 10^4 \times \textit{total volume}$$

Flow cytometry acquisition

After preparing the single cell suspension and staining with the conjugated antibody cocktail described above, samples were acquired on the BD LSR II. This flow cytometer is a benchtop four-laser flow cytometer capable of acquiring parameter values for up to 11 colors. The device has fixed-alignment lasers that are angled by mirrors to go through a flow cell to a user-configurable octagon and trigon detector array. Detectors translate the fluorescent signal given by the chosen antibodies into electronic signals. Electronic signals are converted and saved as digital data [8].

To maintain the reproducibility of the experiments, I used sphero ultra particle rainbow calibration kits (sperotech) to maintain the BD LSR II within the same parameter ranges for each experiment. These beads are micron-sized particles that emit fluorescence in every channel of the flow cytometer[9]. The rainbow beads emit well-defined peaks that correspond to different fluorophore intensities. For every experiment, I ensured that the peaks were the same. Any variations in peak read were corrected by altering the voltage of the laser emitter.

2.3 Data preparation

Flow Cytometry analysis

Flow cytometry analyzed using FCS Express version 6 (Denovo Software). The gating strategy included a lymphocyte gate based on forward and side scatter, dead cells excluded based on fixable viability dye and removal of doublets based on forward scatter width and forward scatter height followed by side scatter width and side scatter height. $CD4^+$ populations assessed: Tregs ($CD4^+$,$CD8^-$,TCR-β^+, $Foxp3^+$), naive T cells ($CD4^+$, $CD8^-$, TCR-β^+, $CD44^-$,$CD62L^+$), and activated T cells ($CD4^+$, $CD8^-$, TCR-β^+, $CD44^+$,$CD62L^-$). Replicating cells were identified based on Ki-67 expression. Total cellular numbers were defined using hemocytometer cell counts and flow cytometry data. The gating strategy is shown in (**Fig. 2**)

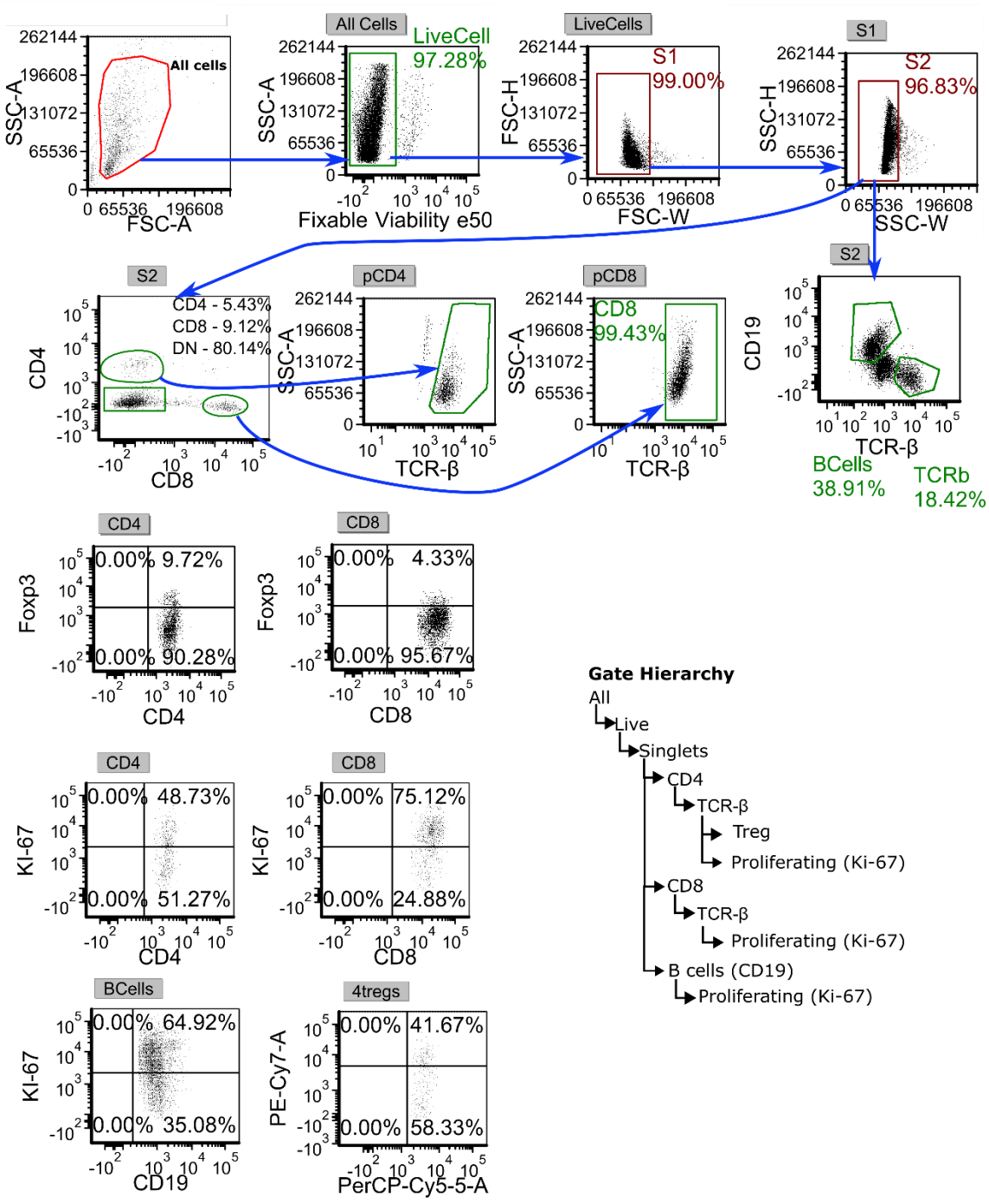

Figure 2. Example of gating strategy. An example of the hierarchical decision making for the selection of gates. Blue arrows indicate the origin of the resulting plot with new variables. Gate hierarchy is shown in the bottom right corner of the figure.

Quantifying cell populations
After data collection, further calculations were performed to quantify populations and sub-populations. Calculations performed and managed use the following code:

Code lists
All code scripts can be in the Hoyer lab box folder, my GitHub account (https://github.com/J-Anzules/HomeostaticExpansion), and if necessary, through e-mail (jonanzule@gmail.com).

- **poCount_V2_AfterPythonScript**
    - **Input:** ActivatedCD4pop2.csv (Raw data results from the batch processing), TCellActivationSummary_filled.csv (Raw data of CD69/CD44/CD62L dataset from Genevieve)
    - **Purpose:** Clean/prep datasets and calculated preliminary cellular ratios.
    - **Output:**
        - *AfterCalculations.csv* - Prepared ActivatedCD4pop2.csv, with incomplete entries and unbalanced experiments
        - *TCellActivationSummary_EdittedinR.csv* - Prepped TCellActivationSummary_filled.csv
        - NaiveTregDifferentiation.csv - Removed incomplete entries and balanced the dataset
- **CalculatingActivatedTCellsFromCD44.py**
    - **Input**: TCellActivationSummary_EdittedinR.csv, NaiveTregDifferentiation.csv
    - **Purpose:** Use groupby methods in Pandas to estimate the activated T cell numbers and combine two datasets
    - **Output**: Cleaned dataset + Estimated Activated T cell ratios
- **poCount_V2_AfterPythonScript**
    - **Input:** Combined data set, with estimated activated T cells and naive T cells.
    - **Purpose:** Last set up before data can be used for model fit.
    - **Output:** Cleaned dataset ready for model fitting

Treg quantification example
Here I present a verbal description of how I quantified the Treg population and its subpopulations: thymic-derived Tregs, naive-derived Tregs, and self-replicating Tregs.

Definitions

Total live cell counts in organ determined using a hemocytometer

Total lymphocyte = Singles and live cells
CD4 T cells = $CD4^+TCR\text{-}\boldsymbol{\beta}^+$
Treg = $CD4^+TCR\text{-}\boldsymbol{\beta}^+ Foxp3^+$
Proliferating Treg = $CD4^+TCR\text{-}\boldsymbol{\beta}^+ Foxp3^+ KI\text{-}67^+$
Thymic Treg ratio = Ratio $CD4^+TCR\text{-}\boldsymbol{\beta}^+ Foxp3^+ KI\text{-}67^+$ in the thymus

Calculations

CD4 ratio = CD4 T cell events / total live cell events
CD4 T cell count = CD4 T cell ratio * total live cell counts in organ
Treg ratio = Treg events / CD4 T cell events
Treg count = Treg ratio * CD4 T cell count
Proliferating Treg ratio = Proliferating Treg events / Treg events
Proliferating Treg count = Proliferating Treg ratio * Treg count
Thymic derived Treg count = Treg count * Thymic Treg ratio
Naive derived Treg count = Treg count - (Thymic derived Treg count + poliferating Treg count)

- Negative values are marked as 0

2.4 Comparing major features of immune development

P-values mentioned in this chapter are the results of a student t-test comparing WT and KO data. This test compares the means of both genotypes at a specific time; p-values lower than 0.05 are statistically significant.

Organ Weight

Comparing the weight of both the spleen and thymus between WT and KO systems, I observed some differences (**Fig 3)**. In the KO mice, I observed a significant increase in thymic size at day 18 (p-value: 0.014). For the spleen, I see a significant difference in size on day 14 (p-value: 0.016) and day 18 (p-value: 0.003). The increased spleen size is a classical sign of lymphoproliferation seen in the IL-2 KO mouse model [2].

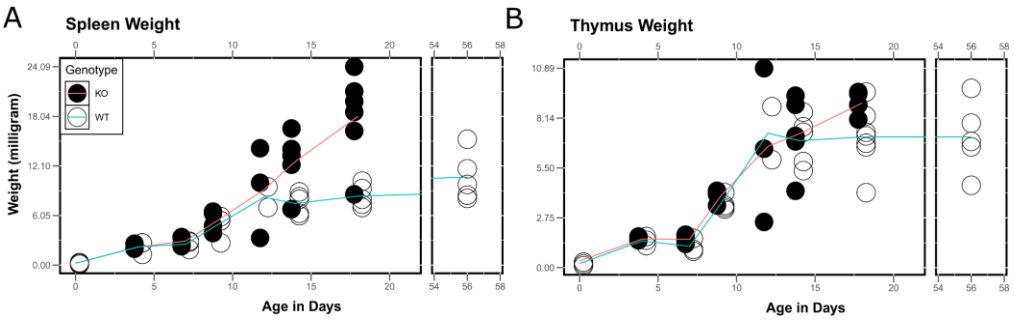

Figure 3. Thymus and spleen organ weights. Closed circles represent KO data, open circles represent WT data. Lines represent the mean of the data points. Both figures show the weight of the organs in milligrams for each experimental takedown day (x-axis). **(A)** Spleen Weight, **(B)** Thymus weight.

Cell populations evaluated

Next, the characterization: CD4 T cells (**Fig 4A**), CD8 T cells (**Fig 4B**), B cells (**Fig 4C**), and CD4 regulatory T cells (**Fig 5**). Data for these populations are from both the spleen (top row) and thymus (bottom row). For total CD4 T cell numbers there is no statistical significance between the genotypes (**Fig 4A**). However, as expected based on prior publications, activated CD4 T cells are increased in KO spleen beginning on day 12 [2,3] (**Fig 6B; section 2.5**). For KO CD8 T cells

(**Fig 4B**) I see a significant increase in population size on day 18 (p-value: 0.008). For KO total B cell numbers, there is a significant increase in cell numbers on day 9 (p-value: 0.027) in the spleen (**Fig 4C**).

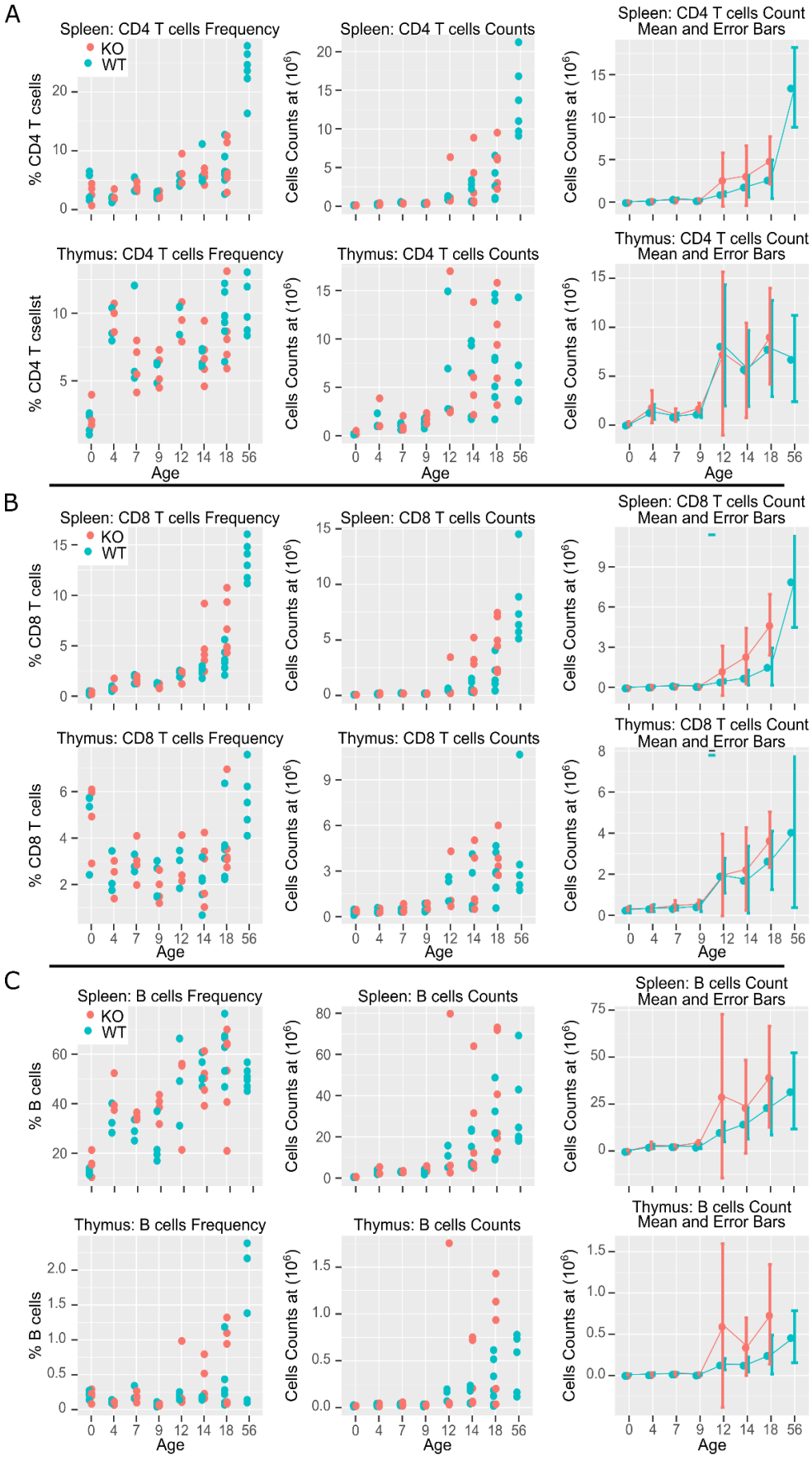
A
Spleen: CD4 T cells Frequency
KO
WT
% CD4 T csells
Spleen: CD4 T cells Counts
Cells Counts at (10^6)
Spleen: CD4 T cells Count
Mean and Error Bars
Thymus: CD4 T cells Frequency
% CD4 T csellst
Thymus: CD4 T cells Counts
Thymus: CD4 T cells Count
Mean and Error Bars
Age
B
Spleen: CD8 T cells Frequency
% CD8 T cells
Spleen: CD8 T cells Counts
Spleen: CD8 T cells Count
Mean and Error Bars
Thymus: CD8 T cells Frequency
Thymus: CD8 T cells Counts
Thymus: CD8 T cells Count
Mean and Error Bars
C
Spleen: B cells Frequency
% B cells
Spleen: B cells Counts
Spleen: B cells Count
Mean and Error Bars
Thymus: B cells Frequency
Thymus: B cells Counts
Thymus: B cells Count
Mean and Error Bars

Figure 4. T and B cell frequencies and counts in the thymus and spleen. Red is the IL-2 KO data, and blue is the WT data. The top row in each section shows data from the spleen, while the bottom is data from the thymus. The first column represents the proportion of cells out of all lymphocytes. The second column represents the calculated total cells and their individual data points for each experiment. The third column is the total cell counts representing the mean and standard error bars of the data. **(A)** CD4 T cells, **(B)** CD8 T cells, **(C)** B cells.

Tregs

All Treg percentages are calculated by finding the ratio of Tregs ($CD4^{+}Foxp3^{+}$) to total CD4 T cells. In the IL-2 KO model, there is an uncontrolled activation and proliferation of the CD4 T cell population (**Fig 6B, Fig 7B**) [2,10], leading to lower Treg percentage numbers due to the lack of IL-2 survival signal (**Fig 5B**).

No statistical significance of the total Treg cell counts is observed (**Fig 5A**). Focusing on the Treg percentages (**Fig 5B**), I performed a right-tailed student t-test comparing the WT to the KO data and observed a statistically significant decrease, in the KO data, for most days(**Fig 5C**) I note that on day 0 I removed the Treg percentage as these are primarily fetal peripheral Tregs, and thymic Tregs do not emerge until day 3-4 [1].

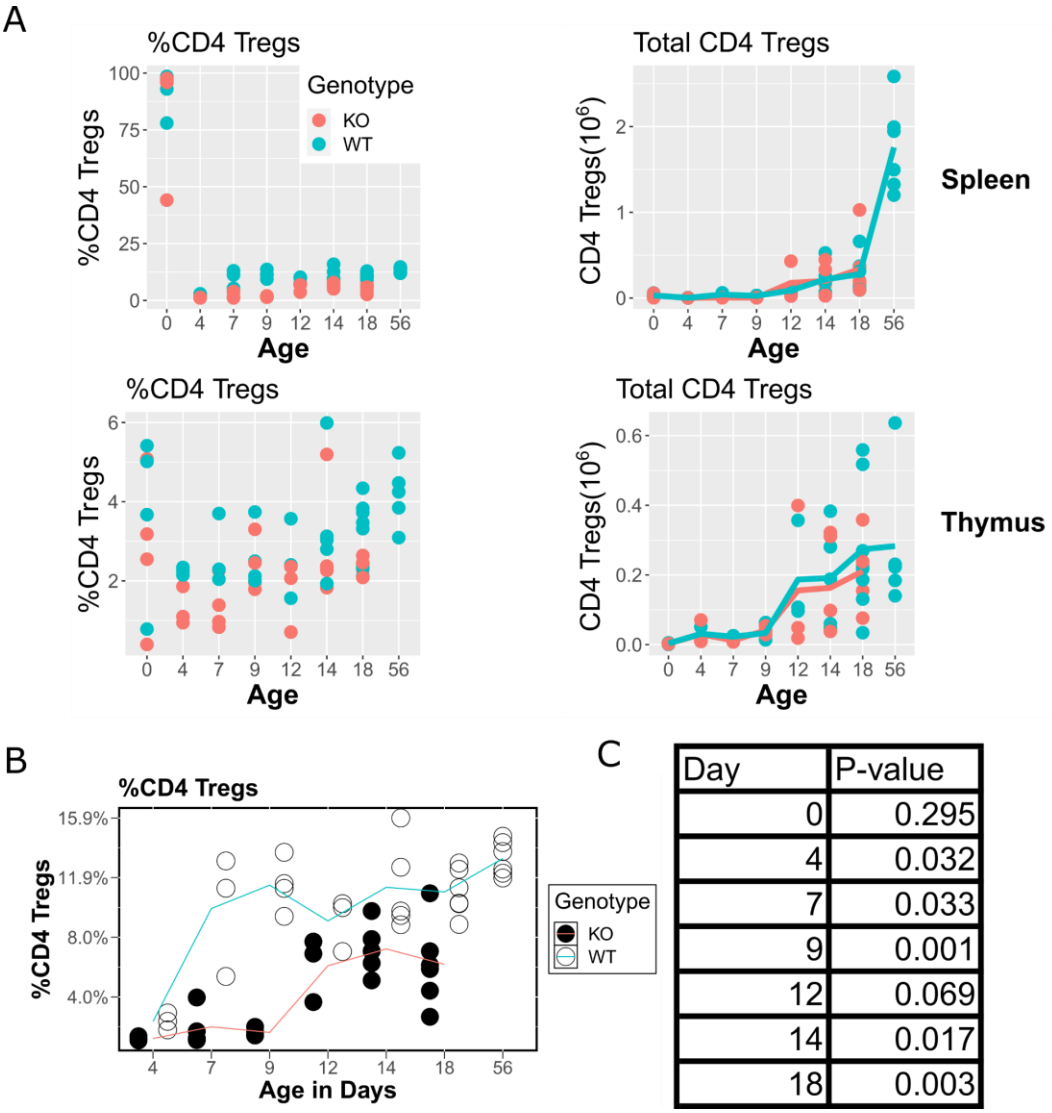

Day	P-value
0	0.295
4	0.032
7	0.033
9	0.001
12	0.069
14	0.017
18	0.003

Figure 5. Characterization of Treg population in the spleen and thymus. **(A)** In red is the IL-2 KO data, and blue is the WT data. The top row shows data from the spleen, while the bottom is data from the thymus. The first column represents the proportion of CD4 Tregs out of all lymphocytes. The second column represents the calculated total cells and their individual data points for each timepoint. The third column is the total cell counts representing the mean and standard error bars of the data. **(B)** Lines represent the mean of the data points. Closed circles represent KO data, open circles represent WT data. **(C)** P-values of a right-tailed student t-test comparing the Treg frequency between WT and KO data.

2.5 Characterization of CD4 T cell subpopulations

I assumed that the Treg ratio in the thymus is the same ratio for how many thymic derived Tregs are in the periphery. I defined naive T cells as $CD4^{+}CD62L^{+}CD44^{-}$ to calculate the amount of naive T cells in the periphery. With the naive T cells calculated, I assume that non proliferating naive T cells ($Ki\text{-}67^{-}$) are thymic derived naive T cells (**Fig 6A**). I define the ratio of $CD4^{+}CD62L^{-}CD44^{+}$ as activated T cells (**Fig 6B**). Total activated T cells in IL-2 KO mice have a significant increase on the day on days 12 (p-value: 0.002), 14 (p-value: 0.009), and 18 (p-value: 0.003). For total activated CD4 T cell count I see a statistically significant increase on day 18 (p-value: 0.01). Ki-67 was used to calculate all of the replicating sub populations (**Fig 6C**); activated T cells (red), naive T cells (green) and Tregs (teal). There is no statistical significance in any of the proliferating subpopulations or the naive T cell total population (**Fig 6D**).

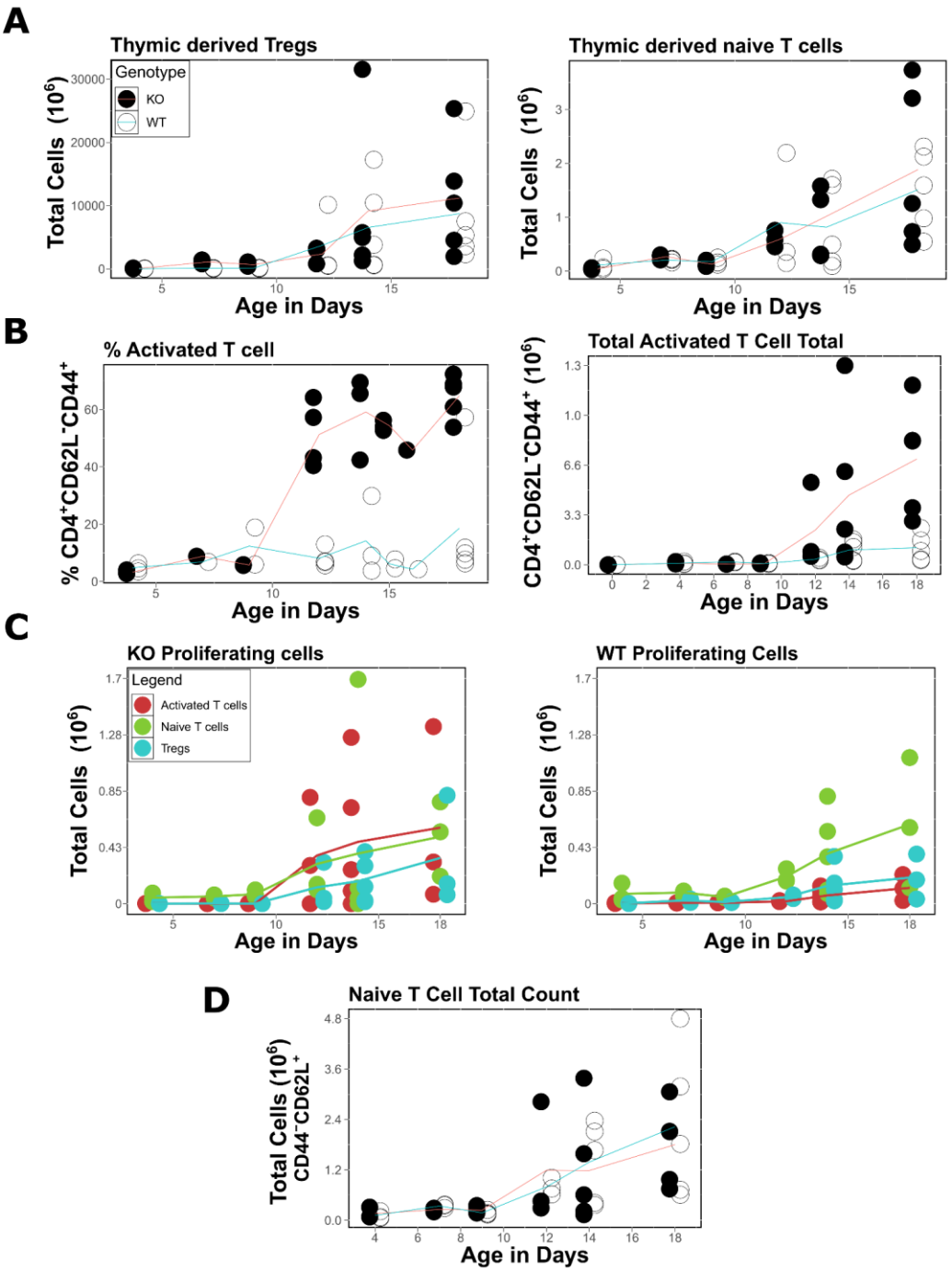

Figure 6. Characterization of T cell subpopulations. (A,B,C) Lines represent the mean of the data points. Closed circles represent KO data, open circles represent WT data. **(A)** Thymic derived Tregs (left) and naive T cells (right). **(B)** Activated T cell percentage (left) and activated T cell total cell count (right) **(C)** Displays all the proliferating populations (activated T cells (red), naive T cells (green) and Tregs (teal)) of WT (left) and KO (right). **(D)** Total naive T cell count.

2.6 Preparing experimental data for mathematical modeling

I focus my project on three CD4 T cell populations: naive T cells, activated T cells and regulatory T cells and structured it as such:

- Total Naive T cells
    - Thymic derived naive T cells
    - Proliferating naive T cells
- Total Activated T cells
    - Naive derived activated T cells
    - Proliferating activated T cells
- Total Regulatory T cells
    - Thymic derived regulatory T cells
    - Proliferating regulatory T cells
    - Naive derived regulatory T cells

In the following plots I present a global view of each population and their respective subpopulations (**Fig 7**). The topmost line of each plot shows the total cell count of all its sub populations (Red). There are no significant differences in the naive T cell population (**Fig 7A**). In the activated T cells data (**Fig 7B**), there are major differences between the WT and KO data that I will try to replicate in my mathematical model (Chapter 3).

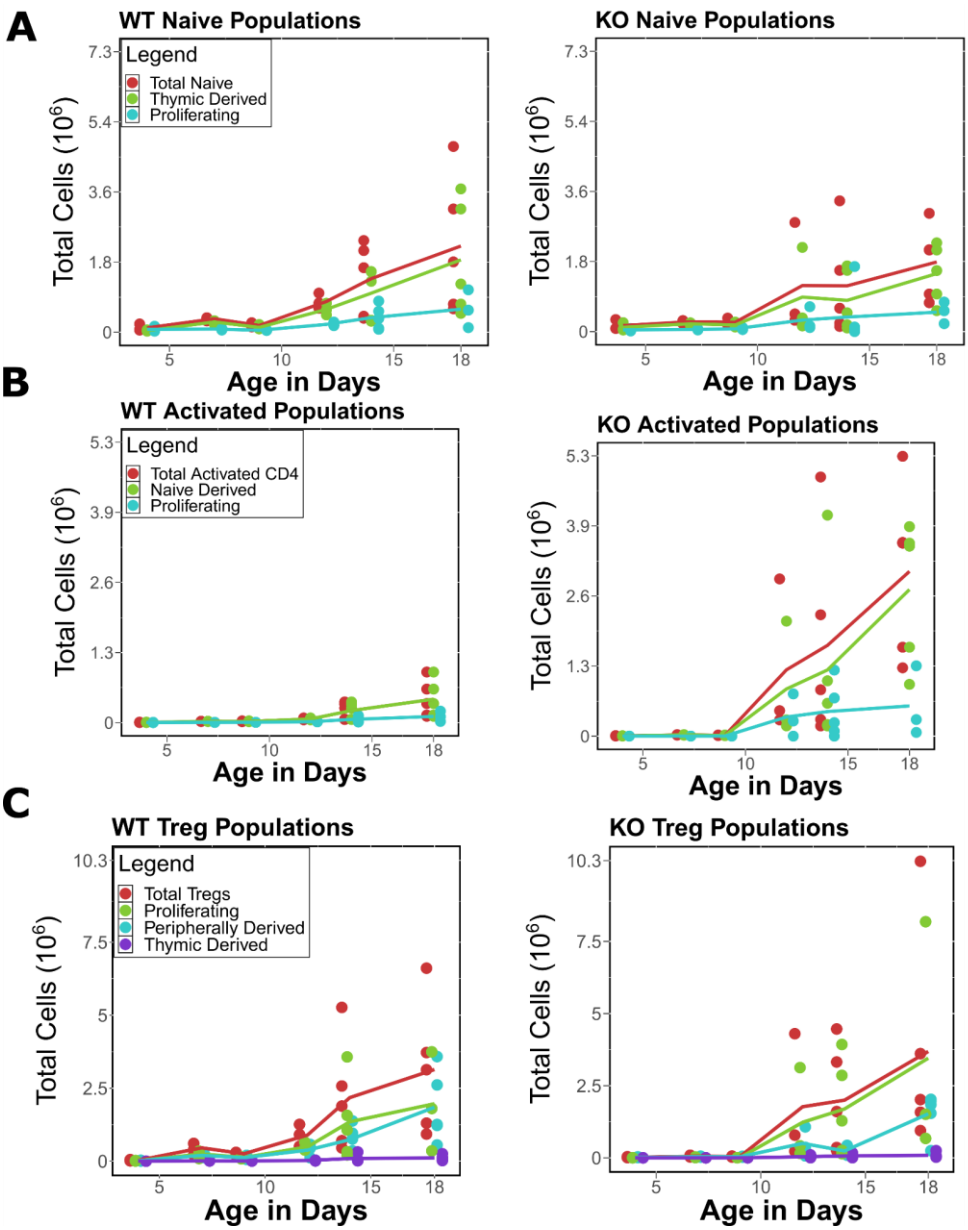

Figure 7. **Global view of naive, activated, and Treg populations.** Circles represent single data points from each experiment, lines represent the mean of those data points for each day. **(A)** Naive T cells population and its sub populations: total naive T cells (red), thymic derived naive T cells (green), proliferating naive T cells (teal). **(B)** Activated T cells and their sub-populations: total activated T cells (red), naive derived activated T cells (green), proliferating activated T cells (teal). **(C)** Tregs and their subpopulations: Total Tregs (red), proliferating Tregs (green), naive/peripherally derived Tregs (teal), and thymic derived Tregs (purple).

The methodology used to develop a mathematical model, fit the model to the data, explore the dysregulation caused by the lack of IL-2 in the KO system, and possible avenues for prevention of autoimmune disease development is explained in Chapter 3.

References

1. Asano, M., Toda, M., Sakaguchi, N., & Sakaguchi, S. (1996). Autoimmune disease as a consequence of developmental abnormality of a T cell subpopulation. *The Journal of experimental medicine*, *184*(2), 387-396.
2. Sadlack, B., Löhler, J., Schorle, H., Klebb, G., Haber, H., Sickel, E., ... & Horak, I. (1995). Generalized autoimmune disease in interleukin-2-deficient mice is triggered by an uncontrolled activation and proliferation of CD4+ T cells. *European journal of immunology*, *25*(11), 3053-3059.
3. Hoyer, K. K., W. F. Kuswanto, E. Gallo, and A. K. Abbas. 2009. Distinct roles of helper T-cell subsets in a systemic autoimmune disease. Blood 113: 389–395.
4. Gravano, D. M., Al-Kuhlani, M., Davini, D., Sanders, P. D., Manilay, J. O., & Hoyer, K. K. (2016). CD8+ T cells drive autoimmune hematopoietic stem cell dysfunction and bone marrow failure. *Journal of autoimmunity*, *75*, 58-67.Valentine, K. M., Davini, D., Lawrence, T. J., Mullins, G. N., Manansala, M., Al-Kuhlani, M., ... & Hoyer, K. K. (2018). CD8 follicular T cells promote B cell antibody class switch in autoimmune disease. The Journal of Immunology, 201(1), 31-40.
5. Mullins, G. N., Valentine, K. M., Al-Kuhlani, M., Davini, D., Jensen, K. D., & Hoyer, K. K. (2020). T cell signaling and Treg dysfunction correlate to disease kinetics in IL-2Rα-KO autoimmune mice. Scientific reports, 10(1), 1-16.
6. Hoyer, K. K., Wolslegel, K., Dooms, H., & Abbas, A. K. (2007). Targeting T cell-specific costimulators and growth factors in a model of autoimmune hemolytic anemia. The Journal of Immunology, 179(5), 2844-2850.
7. Maecker, H., & Trotter, J. (2008). Selecting reagents for multicolor flow cytometry with BD™ LSR II and BD FACSCanto™ systems. Nature Methods, 5(12), an6-an7.
8. Wang, Lili, et al. "Toward quantitative fluorescence measurements with multicolor flow cytometry." Cytometry Part A: The Journal of the International Society for Analytical Cytology 73.4 (2008): 279-288
9. Horak, I. (1995). Immunodeficiency in IL-2-knockout mice. Clinical immunology and immunopathology, 76(3), S172-S173.

Chapter 3

Methods and Results: for developing a mathematical model of autoimmune dysregulation

I quantified and prepared a dataset of the central populations (naive CD4 T cells, activated CD4 T cells, and regulatory T cells) and the subpopulations. In this chapter, I detail the work behind developing a mathematical model and the process of fitting that model to the data collected. With a fit model, I can explore dynamics in silico, which would otherwise be costly if explored from in vivo and in vitro experiments.

There are several biological constraints to be considered during the development of this mathematical model. One of those constraints is the limited supply of IL-2 by activated T cells in the spleen [1]. This IL-2 supply is critical for the survival and maintenance of Treg suppressive function. Interestingly, IL-2 has a seemingly contradictory role: activated T cells supply the IL-2 cytokine to the Treg population, whose role is to suppress the activation of T cells [2]. The relationship between Tregs, activated T cells, and IL-2 implies the presence of a balance between the activation of T cells and their suppression by Tregs. Disruption of this balance can lead to the development of autoimmune disease, as seen in the IL-2 KO mouse model [3].

The data I collected and prepared (Chapter 2) adds more complexity to the story between activated T cells and Tregs. Namely, the supplying force by naïve T cells and thymic production. The thymus can produce naïve T cells and Tregs, while naïve T cells can differentiate into Tregs or activated T cells. With my model, I attempt to encapsulate the dynamics of all these cellular populations in a system that develops autoimmune disease (IL-2 KO) and a healthy one (WT).

Once the model is fit to the data, I will attempt to shed some light to the following questions:

- How early does the lack of IL-2 cytokine start disrupting the immune system?
- What is the global effect caused by the disruption of the IL-2 supply?
- Does the starting population size matter for disease progression?
- Can I quantify the suppressive difference between a healthy and an IL-2 KO autoimmune system?
- How much activation is necessary for healthy immune development?
- Which rates of my model are the most sensitive to disruption?
- What are the best methods for preventing autoimmune disease development?

My aim with this project is to develop a mathematical model that comprehensively studies the dysregulation that occurs in the development of autoimmune disease.

3.1 Model description

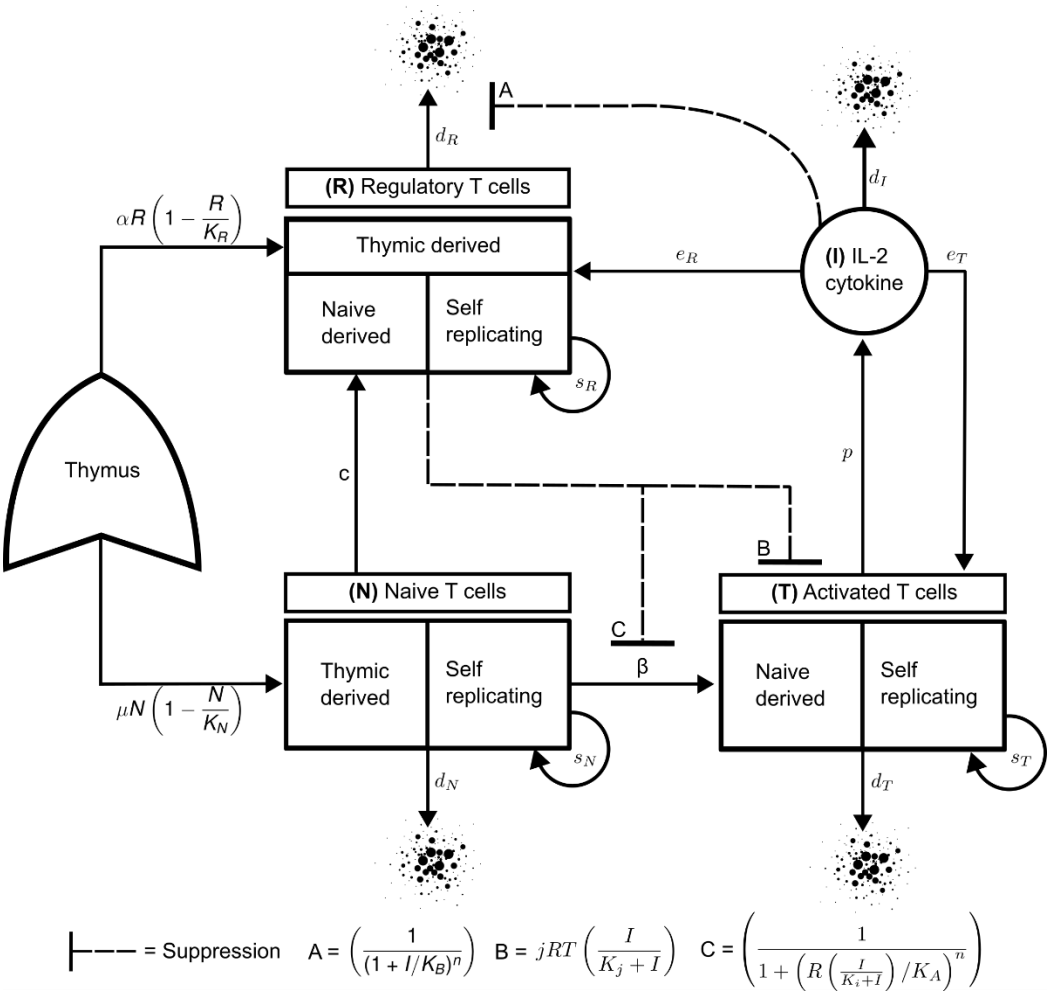

Figure 8. Flow Diagram. Visual representation of my system of ordinary differential equations (equations 1 – 4). Solid line with arrows indicates the flow of cellular and cytokine populations while dashed lines with a bar head represent suppression. The system begins with the supply of naïve T cells and regulatory T cells (Tregs) by their production in the thymus. Naïve T cells differentiate into Tregs at rate $\boldsymbol{c}$ and can become activated T cells at rate β**.** Naive T cells, activated T cells, and Tregs have their own self replication rate (s_N, s_T, s_R) and death rate (d_N, d_T, d_R). IL-2 cytokine (produced by activated T cells at rate p) is consumed by Tregs at rate e_R and activated T cells at rate e_T. **A, B,** and **C** are terms that are influenced by the presence of IL-2 to inhibit the death rate of Tregs ($\boldsymbol{d_R}$), inhibit naive T cell activation rate (β), and increase the deactivation rate of activated T cells (T). The only difference I have between WT and IL-2 KO simulation is the production rate of IL-2 (p). In the WT, p is set to be 1000 molecules per cell per hour, for the IL-2 KO model it is set to be 100 molecules per cell per hour.

$$\frac{dN}{dt} = \mu N\left(1 - \frac{N}{K_N}\right) + s_n N - \beta N/\left(1 + \left(R\left(\frac{I}{K_i+I}\right)/K_A\right)^n\right) - d_N N \quad (1)$$

$$\frac{dT}{dt} = \beta N/\left(1 + \left(R\left(\frac{I}{K_i+I}\right)/K_A\right)^n\right) + s_T - jRT\left(\frac{I}{K_J+I}\right) - d_T T \quad (2)$$

$$\frac{dR}{dt} = \alpha R\left(1 - \frac{R}{K_R}\right) + s_R + cN - d_R/(1 + I/K_B)^n \quad (3)$$

$$\frac{\mathrm{dI}}{\mathrm{dt}} = pT - \mathrm{e_T}IT - \mathrm{e_R}IR - \mathrm{d_I}I \quad (4)$$

Khailaie et al. developed a mathematical model concluding that the discrimination between self and non-self antigens within our bodies is determined by the dynamical structure of the immune system and flow rate of cells between compartments [4]. I modified and expanded on their model to comprehensively study the dysregulation caused by the lack of IL-2 cytokine.

The constant rate of thymic-derived Tregs (R) and naïve T cells (N) cells did not well match my data. As I explored other options, I found that a model where the rate at which naïve and Tregs exit the thymus depends on the population outside of the thymus works best. I assume that the rate at which Tregs and naïve T cells exit the thymus (α and μ) depends on the population outside the thymus. Specifically, I assume that there is a carrying capacity for the populations ($\mathrm{K_N}, \mathrm{K_R}$) and that as the population approaches it the rate from the thymus goes to 0. The thymic production of naïve T cells is represented by $\mu N(1 - N/K_N)$ and thymic Treg production by $\alpha R(1 - R/K_R)$.

The naive T cell population can further supply the Treg population by differentiation (c). Naive T cells interact with a combination of antigens from self and microflora. Some of these interactions result in activation and differentiation into activated T cells (T) by a rate of (β). Naïve T cells, activated T cells, and Tregs can self-replicate (s_N, s_T, s_R)**.** All compartments have their own death rate ($\mathrm{d_N}$, $\mathrm{d_R}$, $\mathrm{d_T}$**)** and half-life ($\mathrm{d_I}$).

IL-2 is primarily produced by activated T cells (p) [5], which is then consumed at a constant rate by Tregs ($\mathrm{e_R}$) and activated T cells ($\mathrm{e_T}$). Treg size, homeostasis, and expansion are dependent on the availability of IL-2. Survival and function are also reliant on the presence of IL-2 for Tregs (Setoguchi, 2005). In my model the Treg death rate ($\mathrm{d_R}$) is suppressed by the hill suppressive function

$$\left(\frac{1}{(1 + \mathrm{I}/\mathrm{K_B})^{\mathrm{n}}}\right).$$

I assume that an increase in IL-2 availability (I) will proportionally suppress the death rate of Tregs, $\mathrm{K_B}$ establishes the half suppression rate of the Treg death rate.

Suppression of the activated T cell population is a key feature of the Tregs in my model. Tregs can modulate the function and/or maturation of dendritic cells (DC) [6, 7]. DCs are a type of antigen-presenting cells whose main function is to process antigenic material and present it on the surface for T cells to interact and identify. In my model naïve T cell activation by DCs is represented by a constant rate β. Suppression of naïve T cell activation by Tregs is represented by the term

$$\left(1 + \left(R\left(\frac{I}{K_i+I}\right)/K_A\right)^n\right),$$

where K_A and K_i set the threshold for the regulatory influence on naïve T cell activation by Tregs and IL-2, respectively. Tregs also possess cytotoxic properties by the differential expression of granzymes B, and perforin [8 – 10]. I represent this suppressive functionality by

$$\mathrm{jRT}\left(\frac{\mathrm{I}}{\mathrm{K_j} + \mathrm{I}}\right),$$

where K_j is the half promotion rate by IL-2 and j is the deactivation rate.

For this project I will simulate the behavior of both the WT and IL-2 KO systems. The IL-2 KO mouse model produces no IL-2 cytokine. However, Tregs can supplement other cytokines for its survivability and functionality by the consumption of IL-10 and IL-15 [11, 12]. To represent this functionality, I reduce the production of IL-2 to 10% of the WT value in the IL-2 KO simulation see table 1). This is the only difference between the WT and IL-2 KO simulations.

Parameter definitions

Thymus Production:

- $\boldsymbol{\mu}\left(\frac{cell}{hour}\right)$: Naive T cell production rate from thymus
- $\boldsymbol{\alpha}\left(\frac{cell}{hour}\right)$: Treg production rate from thymus
- nK (*cells*): Carrying capacity of naive T cells
- rK (*cells*): Carrying capacity of Tregs

Self-replication rates

- $S_N\left(\frac{1}{hour}\right)$: Naive T cell self replication rate
- $S_T\left(\frac{1}{hour}\right)$: Activated T cell self replication rate
- $S_R\left(\frac{1}{hour}\right)$: Treg self replication rate

Naive T cell differentiation rates

- $c\left(\frac{1}{hour}\right)$: Naive differentiation to Tregs
- $\boldsymbol{\beta}\left(\frac{1}{hour}\right)$: Naive activation to activated T cells

Suppression dynamics

- *n* (unitless): Hill coefficient
- K_A (*cells*): Treg half saturation rate for suppression of activation ($\boldsymbol{\beta}$)
- K_i (*molecules*): IL-2 50% maximal response for activation suppression
- $j\left(\frac{1}{cells}\right)$: Deactivation rate of activated T cells by Tregs
- K_j (*molecules)*: IL-2 50% maximal response for activated T cell deactivation
- K_B (*molecules*): IL-2 half saturation for suppression of Treg death rate

IL-2 cytokine expression and use

- p $\left(\frac{molecules}{cells \cdot hour}\right)$: T cell production rate of IL-2
- e_T $\left(\frac{1}{cells \cdot hour}\right)$: Activated T cell consumption rate of IL-2
- e_R $\left(\frac{1}{cells \cdot hour}\right)$: Tregs consumption rate of IL-2

Death Rates

- d_N ($\frac{1}{hour}$): Naive T cell death rate
- d_T $\left(\frac{1}{hour}\right)$: Activated T cell death rate
- d_R $\left(\frac{1}{hour}\right)$: Treg death rate
- d_T $\left(\frac{1}{hour}\right)$: IL-2 cytokine half life

3.2 Parameter estimation

Nonlinear least square method

Fitting the mathematical model to the data is a type of regression analysis where the methodology employs the nonlinear least squares method. The nonlinear least-squares analysis is a collection of numerical algorithms that can be utilized to determine the optimal parameter sets for the experimental data. The processes generally consist of an algorithm that employs an initial approximation of the parameters to produce a more accurate approximation. These improved responses are then utilized as beginning approximations in the subsequent iteration to produce an even more accurate approximation. Finally, this procedure is repeated until the approximation yields a stable set of responses (See: Stabilization of Error and parameter ranges) [13].

Each iteration brings us closer to a better representation of my data. At a certain point, a change in parameter selection results in diminishing returns and sometimes even worse results from my simulation; this point I define as the local minimum of errors. I calculate the error between each data point and simulation to quantify the model's behavior relative to the experimental data. A reduction in error values defines a better approximation of the model. The local minimum is where the calculated error can no longer be lowered by altering parameter ranges.

I am seeking to capture the developmental trajectory of expanding cellular populations (Fig. 7). If I computed the errors without normalizing, resultant values would have a different meaning at earlier time points than later because of the difference in population size. The relative squared error allows me to normalize the error values for all time points. Thus, the errors are calculated by the following objective function:

$$\Omega = \sum_{g=1}^{G} \sum_{b=1}^{B} \sum_{i=1}^{L} \left(\frac{S_{gbi} - D_{gbi}}{S_{gbi}} \right)^2 .$$

my objective function quantifies the relative error value between the simulation output (**S**) and my cellular data **(D**) for each genotype:

G = [WT and IL-2 KO]

Cellular populations:

B = [Total naïve T cells, proliferating naïve T cells, thymic derived naïve T cells,
Total activated T cells, proliferating activated T cells, naïve derived activated T cells,
Total Tregs, proliferating Tregs, thymic derived Tregs, naïve derived Tregs]

and at each time point:

l = [Day 4, 7, 9, 12, 14, 18]

Parameter ranges were estimated by optimizing my parameter ranges to minimize the objective function.

Optimization Minimization Algorithm

Fmincon [14, 15] is a constrained nonlinear optimization algorithm that searches for the best parameter sets that will minimize the error between model output and experimental data. The error is calculated by the objective function mentioned above. The optimization process begins with declaring a parameter range to be tested, and randomly selecting a value within that range. For instance, the self-replication rate of naïve T cells (s_N) is between $2.25e^{-2}$ and $3.20e^{-2}$, the initial parameter value is chosen randomly within this range, in this case: $2.89e^{-2}$. The initial step is done for all parameters in table 2. Then the initial parameter values and ranges are supplied to fmincon, which executes the objective function. The objective functions' code utilizes all equations to obtain simulation results, which are then used to compute the total squared relative error.

Depending on the simulation result and the errors calculated, fmincon will either increase or decrease the parameters given within their respective ranges. As fmincon continues to alter parameter values, it eventually finds a parameter set that produces the smallest possible error. Due to the random nature of this optimization process, it is conducted many times for all parameters. Parameter values determined by fmincon are then saved along with the resultant errors.

The accumulation of data from fmincon can be used to study the relationship between selected parameter values and errors computed (Fig. 9). Additionally, the residuals (errors) from parameter sets can be visualized (Fig. 10). The analysis of simulation results, the relationship

between errors and parameter values, and residuals all help with the decision to either constrain, expand, or shift a parameter range to better represent the experimental data more accurately. Every alteration of parameter ranges improves fmincon's ability to converge on a local minimum of errors, identifying the parameter values that best represent the data.

This optimization minimization process has led me to conclude that the parameter ranges in table 2 are the best representation of the experimental data. Therefore, the only possible way to improve my simulation results would be to alter the structure of the mathematical model (see section 4.2).

Parameters	Description	Range (min, max)	Units
μ	Rate of Naive T Cells from Thymus	$3.90e^{-1}$, $4.07e^{-1}$	hour^{-1}
S_N	Self replication rate of naive T cells	$2.25e^{-2}$, $3.20e^{-2}$	hour^{-1}
$\boldsymbol{\alpha}$	Rate of Tregs from Thymus	$3.50e^{-4}$, $7.00e^{-4}$	hour^{-1}
c	Rate of Naive to Tregs	$1.3e^{-3}$, $1.5e^{-3}$	hour^{-1}
S_R	Treg self replication	$1.0e^{-3}$, $6.0e^{-3}$	hour^{-1}
$\boldsymbol{\beta}$	Rate of Naive to Activated T Cells	$3.00e^{-1}$, $3.13e^{-1}$	hour^{-1}
S_T	Activated T cells self replication rate	$6.4e^{-3}$, $6.8e^{-3}$	hour^{-1}
nK	Carrying Capacity for naive T cells	$1.70e^{6}$, $2.08e^{6}$	cells
d_N	Naive T Cell Death Rate	$9.4e^{-2}$, $10.0e^{-2}$	hour^{-1}
d_R	Treg Death Rate	$0.50e^{-2}$, $1.50e^{-2}$	hour^{-1}
d_T	Activated T cell death rate	$3.7e^{-2}$, $4.43e^{-2}$	hour^{-1}
j	Deactivation rate of ActT by Tregs	$2.25e^{-7}$, $4.18e^{-7}$	cells^{-1}
K_A	Half activation suppression rate by Tregs	$1.61e^{-5}$, $2.68e^{-5}$	cells
K_i	Half rate for activation suppression boost	$2.00e^{-2}$, $3.80e^{-2}$	molecules
K_j	Half rate of deactivation boost	0.36 , 6.80	molecules
K_B	Half suppression of Treg death rate	0.43 , 8.08	molecules

Table 2. Parameter ranges found from the least squares method.

Parameters	Description	Value	Units	Reference
d_I	IL-2 cytokine half life	1.39	$hour^{-1}$	[21-24]
p	IL-2 expression rate	1000, 100 (KO)	$\frac{molecules}{cells \cdot hour}$	[25, 26]
e_T	IL-2 Consumption Rate by Activated T Cells	100	$cells^{-1}$ x $hour^{-1}$	[27]
e_R	IL-2 Consumption Rate by T Regulatory Cells	200	$cells^{-1}$ x $hour^{-1}$	[27]
n	Hill Coefficient	1	-	Fixed
d_{KO}	KO: IL-2 expression rate	100	-	Fixed
rK	Carrying capacity for Tregs	$1.05e^6$	cells	Mean of day 56 $CD4^+Foxp3^+Ki67^-$ cells

Table 3. Fixed parameters.

Stabilization of Error and parameter ranges

Most errors fall between $\Omega = 2665$ (- 1 standard deviation) and $\Omega = 4197$ (+ 1 standard deviation), as found by the optimization procedure. The determination of parameter ranges is evaluated on the stability of fmincon's parameter value output. Therefore, I examined the relationship between the parameter values selected and the resulting errors. A near linear correlation (R-value < 0.3) defines a stability of errors (Fig 9). In addition, I ensured that, within the specified parameter ranges, there was no significant clustering of parameter values near the range's boundaries.

Figure 9 represents a scatter plot of parameter values (x-axis) and their associated errors (y-axis). The plot was generated from 638 iterations of my optimization algorithm. All these plots display a nearly linear relationship (R-value < 0.3) to the errors produced and no significant clustering of parameter values at the edges of their range.

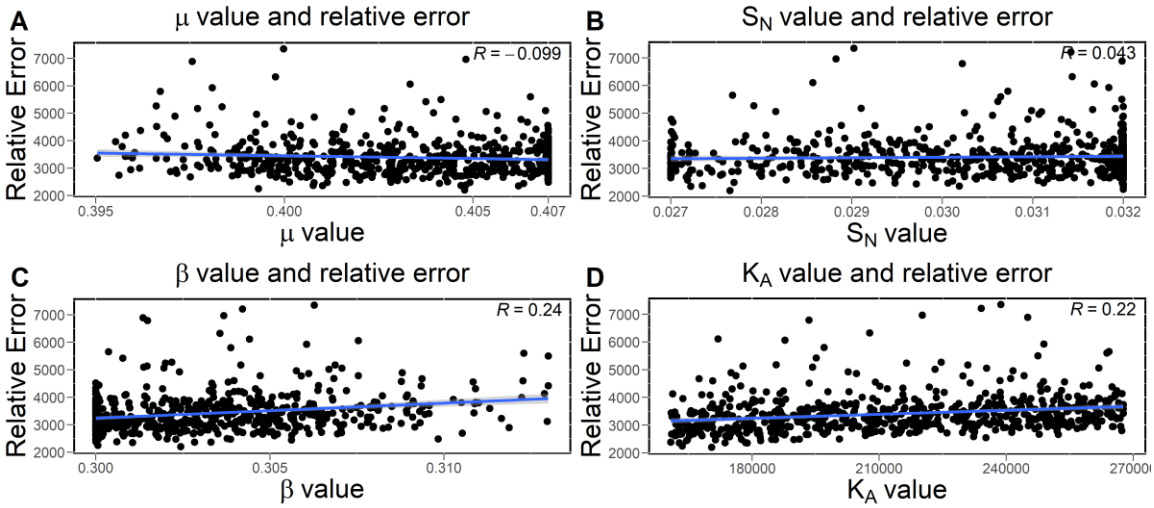

Figure 9. **Results from fmincon parameter estimation search.** Each data point represents one resolution of my optimization algorithm (632 total). The x-axis represents the parameter value, while the y-axis represents the error value of each data point. The blue line in the scatter plot represents the line of best fit determined through linear regression analysis. The top right of each figure shows correlation value. **(A)** μ: thymic naïve T cell production rate **(B)** s_N: naïve T cell self-replication rate **(C)** β: naïve T cell activation rate **(C)** K_A: half suppression rate of naïve T cell activation rate.

Residuals

In addition to selecting parameter ranges by a stable distribution of errors, I looked at the residuals from my model. In statistical, machine learning, or mathematical models' residuals are the differences between predicted and observed values (simulation – experimental data). They serve as a diagnostic tool for evaluating the goodness of fit of the mathematical model. Residuals can also be used to identify patterns or structure in the data that are not explained by the model, which can lead to new insights or hypothesis.

If all residuals are zero, then the simulation represents the data perfectly. However, zero residuals of a model are uncommon with highly varied biological data. In figure 10, the blue line of each figure represents the zeroth value of errors. I searched for an even spread between negative and positive values in my residual spread; this would be a good representation of the data.

Based on the mean error value (3431; table 4), I selected the representative parameter set for the following figures (Figs. 10–16). The scatter plots in Figure 10 are from the residuals of the parameter set I selected. These figures display the data and simulation results (top) along with the corresponding residuals (bottom). The populations plotted are the total naïve T cells, activated T cells and Tregs. Except for the WT activated T cells (Fig. 10B), most of the residuals show a good representation of the data.

Parameters	Description	Value	Units
μ	Rate of Naive T Cells from Thymus	$4.00e^{-1}$	hour^{-1}
S_N	Self replication rate of naive T cells	$2.9e^{-2}$	hour^{-1}
$\boldsymbol{\alpha}$	Rate of Tregs from Thymus	$6.23e^{-4}$	hour^{-1}
c	Rate of Naive to Tregs	$1.4e^{-3}$	hour^{-1}
S_R	Treg self replication	$3.8e^{-3}$	hour^{-1}
$\boldsymbol{\beta}$	Rate of Naive to Activated T Cells	$3.0e^{-1}$	hour^{-1}
S_T	Activated T cells self replication rate	$6.5e^{-3}$	hour^{-1}
nK	Carrying Capacity for naive T cells	$1.81e^{6}$	cells
d_N	Naive T Cell Death Rate	$9.57e^{-2}$	hour^{-1}
d_R	Treg Death Rate	$1.15e^{-2}$	hour^{-1}
d_T	Activated T cell death rate	$4.23e^{-2}$	hour^{-1}
j	Deactivation rate of ActT by Tregs	$4.18e^{-7}$	cells^{-2}
K_A	Half activation suppression rate by Tregs	$2.61e^{5}$	cells
K_i	Half rate for activation suppression boost	$2.3e^{-1}$	molecules
K_j	Half rate of deactivation boost	1.84	molecules
K_B	Half suppression of Treg death rate	0.44	molecules
d	IL-2 cytokine half life	1.39	hour^{-1}
p	IL-2 expression rate	1000, 100 (KO)	$\frac{molecules}{cells \cdot hour}$
e_T	IL-2 Consumption Rate by Activated T Cells	100	cells^{-1} x hour^{-1}
e_R	IL-2 Consumption Rate by T Regulatory Cells	200	cells^{-1} x hour^{-1}
n	Hill Coefficient	1	-
d_{KO}	KO: IL-2 expression rate	100	-
rK	Carrying capacity for Tregs	$1.05e^{6}$	cells

Table 4: Representative parameter values.

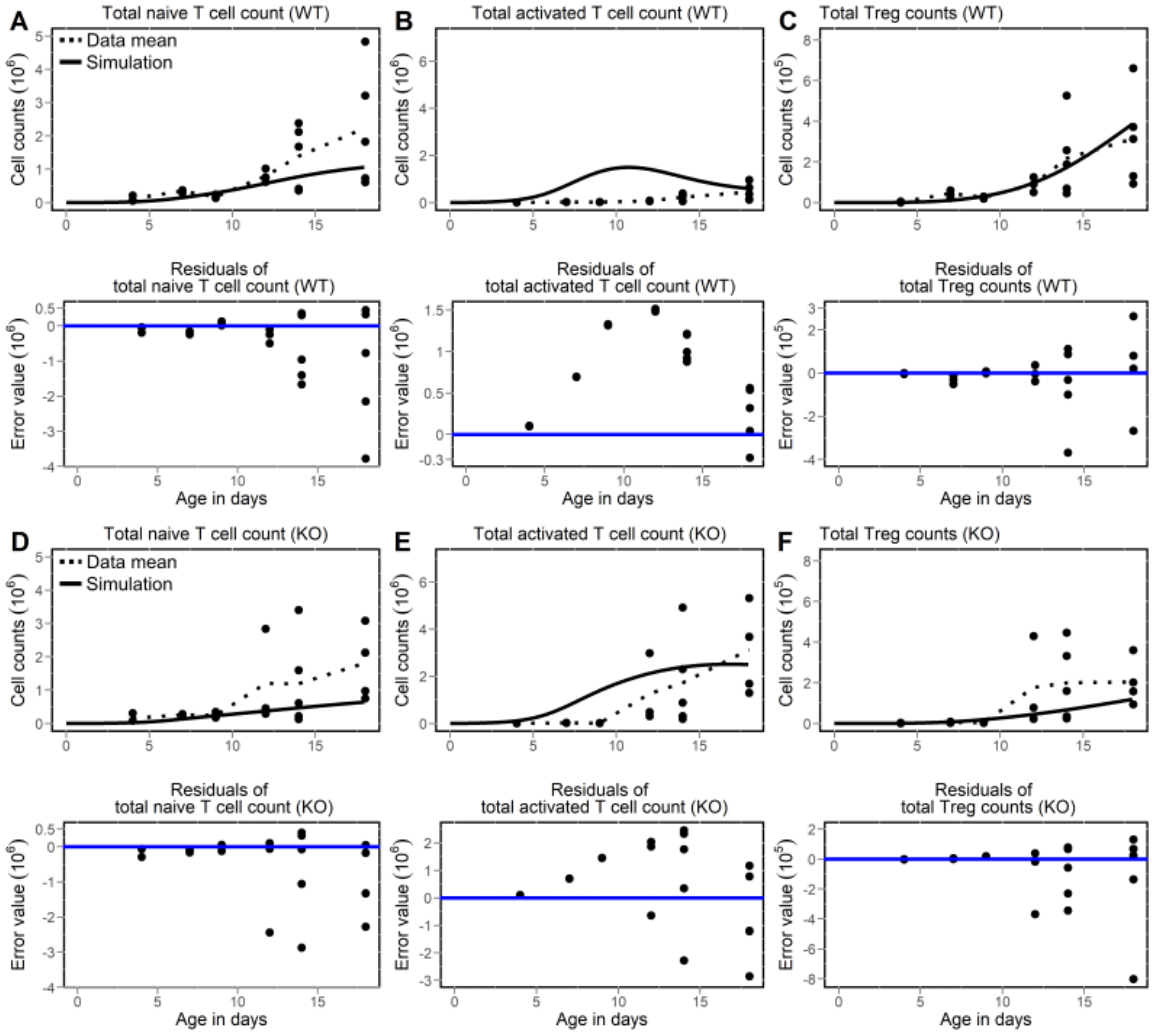

Figure 10. **Residuals and model output from representative parameter set.** Each section of the figure contains the result of my simulation and comparison to the data (top) and the residuals of the model (bottom). The top figure contains the experimental results (black dots), the mean of data points (dotted line), and simulation results (solid black line). The bottom figure contains the residuals (black dots) and the 0 line (blue line). **(A-C)** WT data. **(D-F)** IL-2 KO data. **(A, D)** Total naïve T cells. **(C, E)** Total activated T cells. **(D, F)** Total Tregs.

Beginning on day 12, KO mice had significantly higher activated T cell data than WT mice (Fig. 6). The primary goal of my mathematical model was to replicate this distinction in activated T cell data. Based on comparing the activated T cell simulation results of both genotypes, I could replicate the observed overactivation (Fig. 11B). Unfortunately, my simulation did not accurately reproduce the WT activated T cell data. According to the residuals of WT total activated T cells (Fig. 10B), the residuals are mostly positive instead of an even distribution of positive and negative values. The IL-2 KO simulation, on the other hand, has a better fit for the KO data. The qualitative behavior in activation was accurately captured, but the quantitative was not. Capturing this desired qualitative behavior allows me to investigate the potential dysregulation that must occur prior to autoimmune disease development.

3.3 Result of fit to data

During the early stages of development (days 0 - 9), the growth trajectories between both genotypes are similar in cell numbers. Post day 9 of development all cellular populations transition from the lag phase to exponential growth. On day 12, major differences are seen between genotypes in my data and simulation. My simulations effectively replicate the primary growth patterns of the cellular populations, as depicted in Figure 11. By comparing the results of both WT and KO simulations, I can investigate the dysregulation that occurs in the development of autoimmune disease.

As observed in Figure 11A, a clear distinction in growth patterns among genotypes is evident when analyzing the total naive T-cell populations in my simulation. The growth trajectory of the KO genotype is notably lower compared to that of the WT genotype (Fig. 11A). The decrease of naive T cells suggests that this population is overactivated in autoimmune illness. Examining the activated T cells produced from naïve T cells (Fig. 11B), the KO genotype exhibits a higher level of activation than the WT genotype. These findings suggest that autoimmunity is driven by excessive stimulation of the naïve T cell population. A potential consequence of this in a biological system is that the diversity of naive T cells may decrease, increasing the likelihood that the immune system may not respond effectively to an infection, a condition known as lymphopenia [16, 17].

Figure 11B demonstrates that my simulation accurately reproduced the over activation and proliferation of activated T cells in the KO genotype. However, the model did not accurately reflect the data for the WT simulation, which highlights a limitation of the model. Despite extensive parameter searches, my model was unable to accurately capture both the WT data and the overactivation seen in the KO data. I concluded that only a restructuring of my mathematical model could lead to improved results. Despite this limitation, I will continue to investigate the model as it does capture the qualitative behavior of overactivation in the KO simulation compared to the WT.

In the WT model and data, I noticed the population of activated T cells is maintained mostly by the activation of naive T cells (Fig. 11B). The IL-2 KO follows a similar trend, but both the naive derived activated T cells and self-replicating activated T cells prove to be significantly higher in the IL-2 KO simulation. The overactivation of naïve T cells and the reduction in their numbers may subsequently decrease the pool of available naïve T cells that have the capacity to differentiate into Tregs. A decrease in the availability of Tregs could further exacerbate the dysregulation of autoimmune self-reactive cells. I can see the consequence of over-activation in the naive derived Treg population, where there is a reduced number of Treg differentiation in the KO simulation (Fig. 11C).

From my data and other experiments [18, 19] I note that the homeostatic expansion of Tregs is mostly due to the proliferation of Tregs and differentiation from naive T cells. My model was

able to capture this behavior and can be seen in Fig. 11C. Although the Treg numbers are similar between WT and IL-2 KO mouse model data, I noticed that the total Treg count is lower in the KO simulation. This is a quantitative difference seen in my simulation that may help explain some qualitative dysregulation in an autoimmune system.

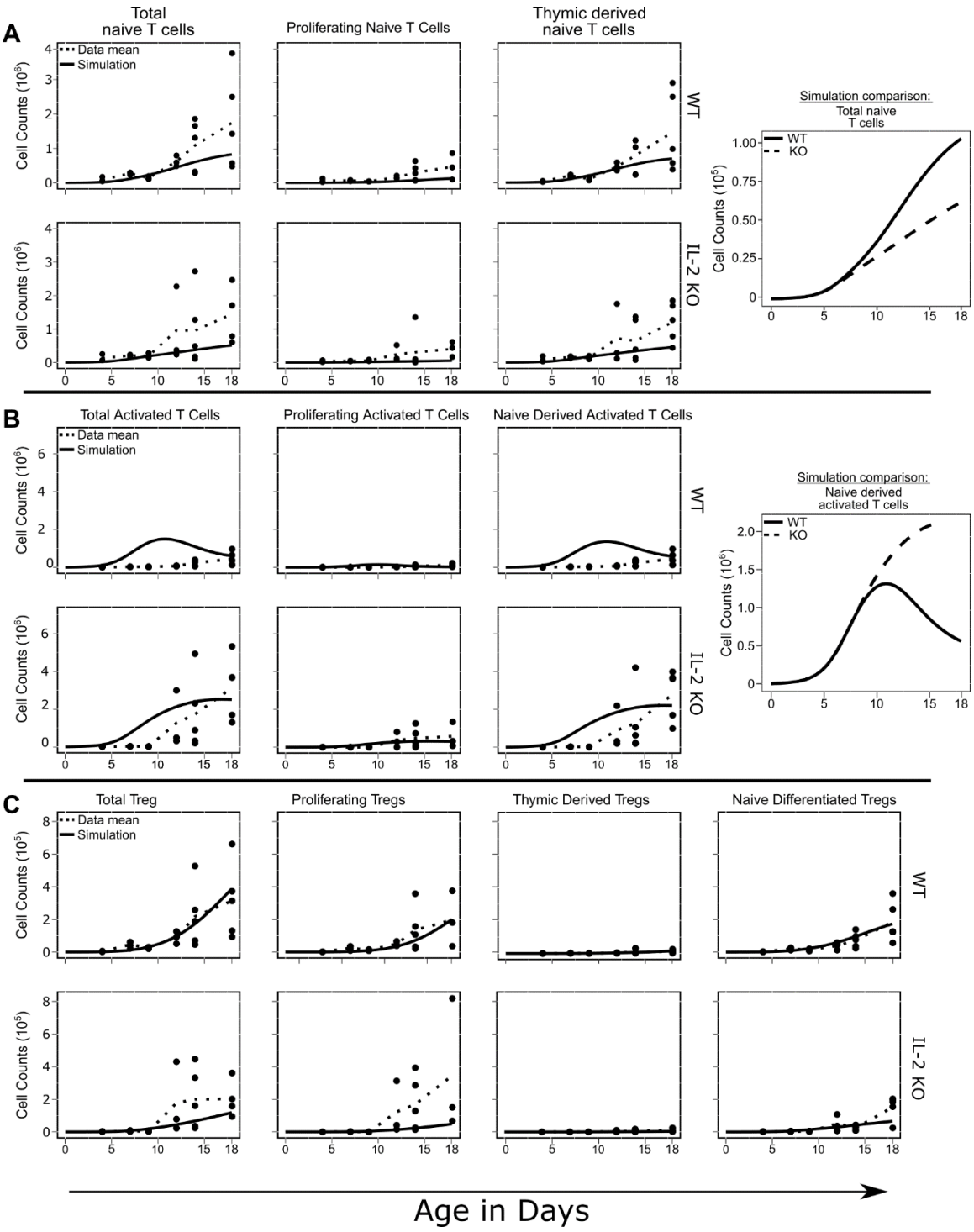

Figure 11. Model fit to data and characterization of homeostatic expansion. All figures contain the results from data collection (black dots), mean of data (dotted line), and simulation results (solid line). **(A-B)** Each section is a table of figures for both WT (top row) and IL-2 KO (bottom row) data and simulation. For the simulation comparisons the WT is represented by a black line and the IL-2 KO by a dashed line. **(A)** Naive T cell population and its sub-populations, starting from the left each column represents the data for total naive T cells, proliferating naive T cells, and thymic derived naive T cells. **(B)** Activated T cell population and its sub-populations, starting from the left each column represents the data for total activated T cell count, proliferating activated T cells, naive derived activated T cells. **(C)** Tregs and their sub-populations, starting from the left each column represents total Treg counts, proliferating Tregs, thymic derived Tregs, naïve derived Tregs.

3.4 Exploring possible dysregulation in the Treg population

I aimed to investigate the dysregulation of the Treg population in the IL-2 KO simulation, as it plays a crucial role in preventing autoimmune disease. Analysis of the Treg population throughout the simulation revealed a reduction at early time points, which becomes more pronounced as the simulation progresses (Fig. 12A). I aimed to uncover the underlying mechanisms of Treg population failure in the IL-2 KO model, which may contribute to the development of autoimmune disease. To achieve this, my algorithm closely monitored the dynamics of the model by focusing specifically on the Treg population. For this section I will focus on parts of the Treg dynamics:

$$\frac{dR}{dt} = \alpha R\left(1 - \frac{R}{rK}\right) + s_R R + cN - d_R R\left(\frac{1}{(1 + I/K_B)^n}\right).$$

I noticed that the Treg death rate, determined by the term: $d_R R/(1 + I/K_B)^n$, is higher in the WT at later time points (Fig. 12B). Because IL-2 deficiency increases Treg mortality, I expected the KO simulations' death rate to be greater throughout the entire simulation. The death rate among Tregs is directly proportional to the overall Treg population size. Thus, as the difference in Treg population size between genotypes increases, so does the number of Treg deaths. Eventually, the disparity in Treg size becomes so great that the WT Treg death rate surpasses that of the KO.

Upon further investigation, the Treg proliferation ($s_R R$) is higher in the WT than the IL-2 KO simulation (Fig. 12C). So, at the same time where Treg death rate is higher in the KO simulation, it is also deficient in the it's self-replication. This decline in proliferating ability in the KO simulations has strong implications that the Treg population is crippled from birth in the KO mouse models. The results of further analysis demonstrate that the self-replication rate of Treg cells in the KO model is insufficient to match the rate observed in the WT (Fig 15D). In later sections I will test the consistency of these patterns by using Latin hypercube sampling (Section 3.5).

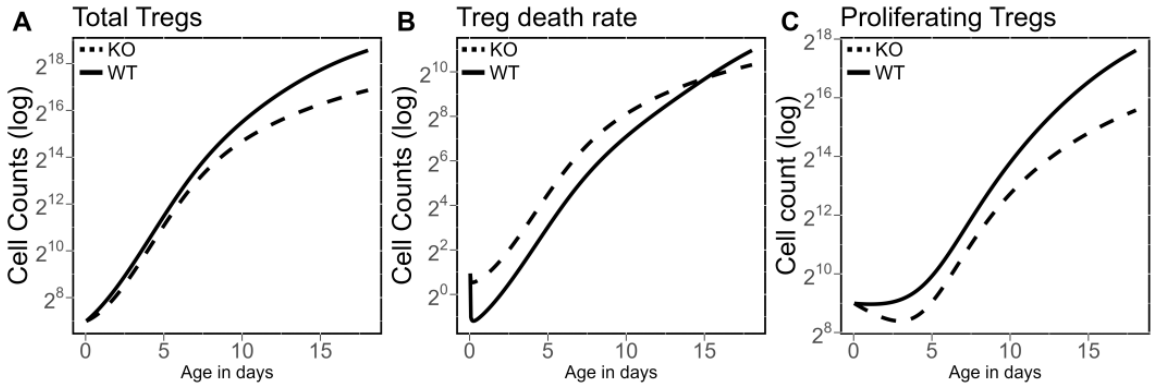

Figure 12. **Comparison of Treg Population Dynamics in Wild-type and Knock-out Simulations: Total Tregs, Death Rate, and Proliferation Rates.** Plots display the Log transformation of various Treg population rates and sizes. The solid lines indicate WT simulations, while the dotted lines reflect KO simulations. **(A)** Total Treg population size **(B)** Treg death rate and **(C)** Treg proliferation rate

3.5 Latin hypercube sampling

Latin hypercube sampling (LHS) is a statistical method used for the sampling of near-random input values from a multidimensional distribution. I used lhsdesign [20] to generate an LHS matrix of size r-by-g; Where r is the number of simulations runs and p is the number of parameters to be tested. The randomized parameter values are obtained from a continuous uniform inverse cumulative distribution function.

I implemented LHS to test the uncertainty of patterns seen in my model. For all experiments, I executed 3000 simulations with a +/- 60% variation of the initial input values. From the tested simulations, I calculated the mean, 10th and 90th percentile of the results for visualization.

Sensitivity Analysis

I performed a first-order sensitivity analysis; I measured the fractional contribution of a single parameter to the model's output variance. I approached this method by taking 3000 LHS for each experiment and sequentially incrementing the parameter ranges; +/- 3%, +/- 10%, +/- 50%, +/- 90%, +/- 99%. I found that μ, thymic production rate of naive T cells; β, activation rate of naive T cells; and d_N , the death rate of naive T cells to be the most sensitive parameters in the system. Figure 13 is the result of +/- 10% LHS sampling of the μ parameter. While figure 14 results from a +/- 90% LHS sampling of parameter α, the thymic production rate of Tregs.

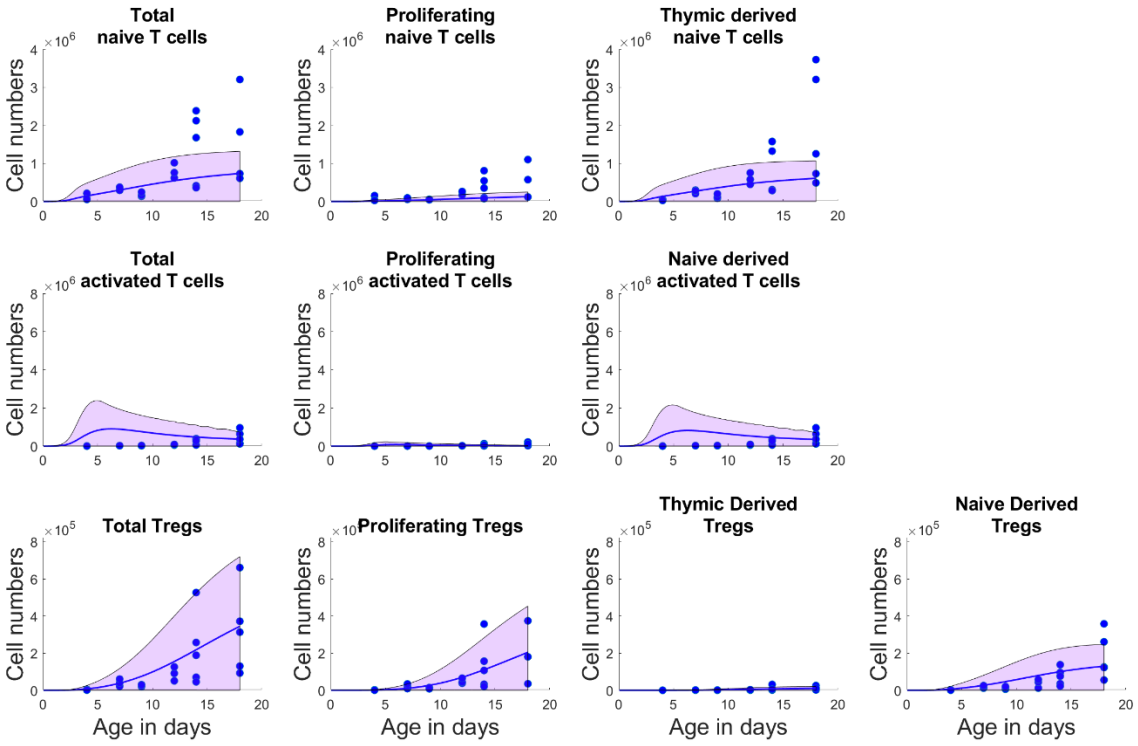

Figure 13. Results of μ sensitivity analysis. First order sensitivity analysis of +/- 10% LHS sampling of the **μ** parameter (thymic production rate of naive T cells). Results show the WT simulation. Blue dots represent experimental data, the top of the filled in area is the 90th percentile result, while the bottom is the 10th percentile mark, the blue line in the middle of the area represents the mean of all the model output.

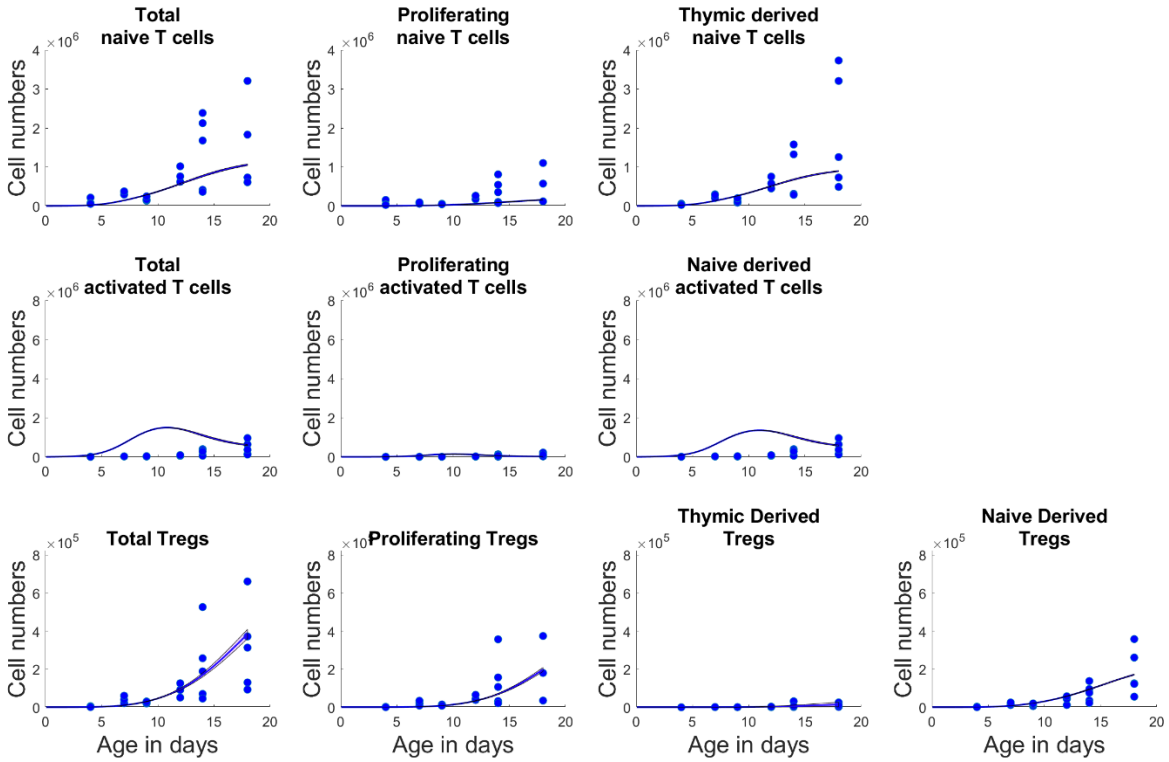

Figure 14. Result of α sensitivity analysis. First order sensitivity analysis of +/- 90% of 3000 LHS sampling of parameter **α**, thymic production rate of Tregs. Results show the WT simulation. No filled in region is clearly seen (No variation).

I also conducted a sensitivity analysis on the initial conditions of the model. A test of a +/- 99% range of the initial conditions displayed similar results to figure 14**.** From this result I can conclude that the model results do not depend on the initial conditions of the model. The continuous production and proliferation of new cells by the thymus suggests that the growth of the cellular population is contingent upon the rate of their production and replication.

3.6 Dysfunction created by IL-2 deficiency

To investigate the stability of deregulatory processes in the KO Treg populations, I utilized the LHS method as a statistical analysis tool [20]. This approach allows us to assess the consistency dysregulation seen in section 3.4. Specifically, I aimed to vary three key parameters that affect Treg survival: the Treg death rate (d_R), the half suppression rate of Treg death rate (k_B), and the IL-2 production rate for WT and KO cells (p and p_{KO} respectively). I varied these parameters between +/- 60% using an LHS algorithm. From those simulations, I calculated the mean, 90th, and 10th percentile for each time point and plotted it (Fig. 15).

In the KO simulation, I observed a decrease in the availability of IL-2 (Fig. 15A). This reduction in IL-2 availability leads to a weaker suppression of the Treg death rate (Fig. 15B). I quantified

the suppression strength of the Treg death rate with the term: $1 - (1/(1 + I/K_B)^n)$. Despite the randomization, the pattern of increased Treg death rate early on persisted (Fig. 15C).

The results of the LHS analysis of the Treg death rate ($d_R R/(1 + I/K_B)^n$) reveal that, over time, the death rate of Tregs in the WT population surpasses that of the IL-2 KO population (Figure 15C, top panel). The increased death rate in the WT population is likely due to the greater number of Tregs present, resulting in a higher rate of deaths per hour. However, during the early stages of development, the IL-2 KO Tregs exhibit a slightly elevated death rate compared to the WT population (Figure 15C, bottom panel).

The variation in the rate of early Treg cell death among different genotypes is important, as it can significantly impact the homeostatic expansion of Treg cells, which is mainly driven by their proliferation. The increased death rate of Tregs during early IL-2 KO mice development may reduce the initial Treg population, reducing the capacity for Treg proliferation and growth (Fig. 15D). Due to these deficiencies, the IL-2 KO Treg population is never able to properly develop (Fig. 15E).

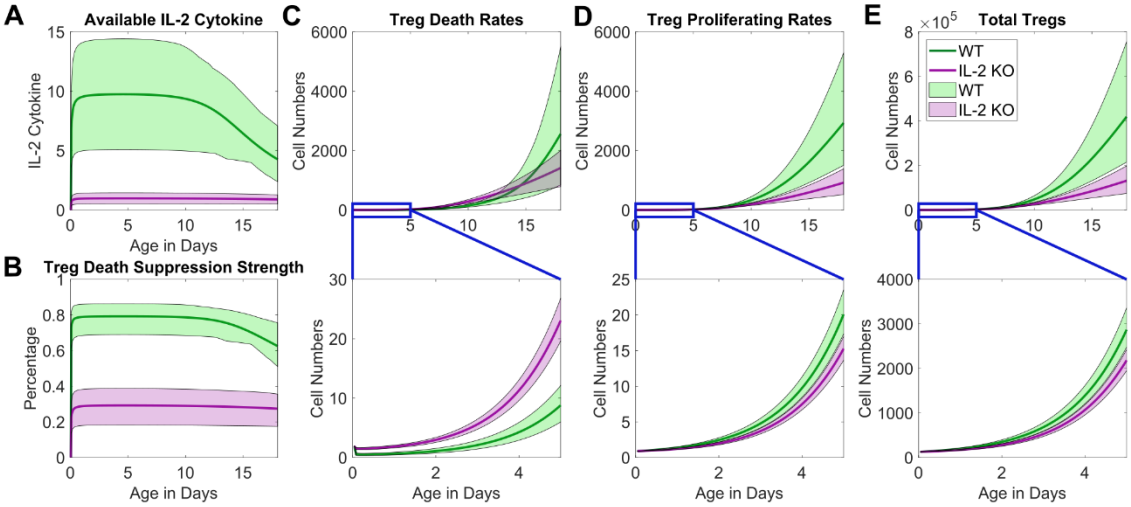

Figure 15. Impact of IL-2 Deficiency on Treg Cell Dynamics: Dysregulation of the Treg populations. Results from the +/- 60% LHS sampling range of parameters: $\mathbf{d_R}$, **p**, $\mathbf{p_{KO}}$, $\mathbf{K_B}$; for 3000 simulations. Chosen parameters affect Treg survival. The shaded represents the range of variability across all simulation results, where the top line corresponds to the 90th percentile, representing the upper limit of the variability, and the bottom line corresponds to the 10th percentile, representing the lower limit of the variability. The solid lines within the shaded region represent the mean, which represents the average value across all simulations. Green represents the wild-type data, while pink represents the IL-2 KO data. **(A)** Available IL-2 cytokine in the system has a deterministic influence on **(B)** Treg death suppression strength. **(C-E)** Below every plot is a zoomed-in view of the data above it. **(C-E)** Represents the instantaneous rates of Treg death **(C),** Treg proliferation**(D),** and total Treg population size **(E)**.

3.7 Prevention of autoimmune disease

Due to the lack of IL-2 cytokine both the Treg population size and suppression are negatively affected. In combination, I set out to quantify the suppressive difference between a healthy and an autoimmune system by preventing autoimmune progression in the KO simulation.
For this section, I assigned KO-specific parameters that directly impact the suppressive functionality of Tregs. Namely, K_{AKO} is the half rate value for the suppression of the activation rate (β); j_{KO}, is the removal rate of activated T cells by Tregs. These parameters have similar mathematical functions as K_A and j in the WT simulation, but their values are not dependent on each other. I set up an LHS experiment for the parameters K_A, j, K_{AKO}, and j_{KO} for the span of 3000 simulations and varied the parameters between +/- 60%. The results of these simulations seek to predict the behavior of the system past the point of data collection (day 18) until day 25.

A variation of +/- 60% in parameters without altering the initial KO-specific parameters clearly shows patterns of over-activation consistent with autoimmune disease (Fig. 16A top). The KO activation (purple) does not exhibit the same level of control as the WT results (green), which are able to be stabilized after the initial activation peak. This difference in activation is what I am defining as autoimmune disease in the KO simulation. I aim to determine the quantitative difference in suppressiveness between the wild-type (WT) and knock-out (KO) systems by comparing the activation suppressive strength as measured by

$$\left(1 - \left(1/(1 + (R\,(I/K_i + I)/K_A)^n)\right)\right)$$

(Fig. 16, middle panel) and the rate of removal of activated T cells as measured by

$$jRT\left(I/K_J + I\right)$$

(Fig. 16, bottom panel). Without the manipulation of KO-specific parameters, the Treg suppressive abilities in the WT are superior during the most critical times of development.

I quantitatively assess the suppressive deficiencies in the IL-2 KO simulation by manipulating the IL-2 KO specific parameters (K_{AKO}, and j_{KO}) to determine the extent to which these parameters must be adjusted to produce results like those of a healthy system. When I increase the j_{KO} parameter by 300% I notice that the rate of activation is lower (Fig. 16B top) than no change (Fig. 16A top), but not quite to the level of WT. Even with the high variation of parameter values and tripling of the j_{KO} parameter I was not able to control the over-activation in autoimmune disease. The strength of suppression and the rate of naive T cell activation did not improve during the critical developmental stages.

Reducing the half suppression rate (K_{AKO}) by 83%, thus increasing the effectiveness of suppression of activation, I noticed the out-of-control activation is brought under control in the KO simulation and now overlaps with the WT (Fig. 16C top). Suppression strength and removal of activated T cell rate are now greater in the KO system than in the WT during the critical times of development, precluding autoimmune disease. Interestingly, when I artificially reduced the death rate of Tregs in the KO simulation, no significant change in model behavior was detected (not shown).

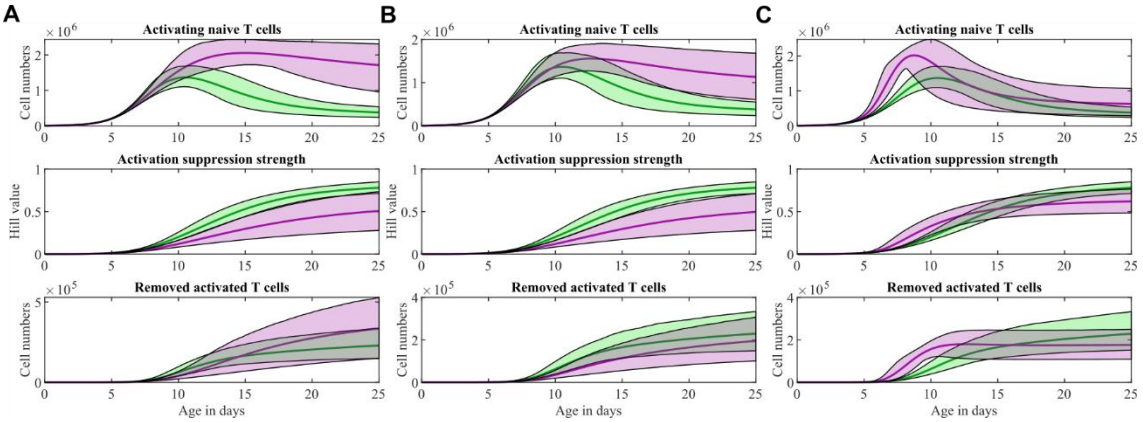

Figure 16. Model prediction and prevention of autoimmune disease. Results from the +/- 60% LHS sampling range of parameters: $\mathbf{K_A}$, $\mathbf{K_{AKO}}$, **j**, $\mathbf{j_{KO}}$, $\mathbf{d_R}$; for 3000 simulations. Parameters with the 'KO' subscript has been edited on the IL-2 KO version of the model to find the best methodology to prevent autoimmune disease. The top figures are activating naive T cells, mid: activation suppression strength, bottom: removed effector cell. I look at the simulation past the point where I have data (day 18) all the way until day 25. The shaded represents the range of variability across all simulation results, where the top line corresponds to the 90th percentile, representing the upper limit of the variability, and the bottom line corresponds to the 10th percentile, representing the lower limit of the variability. The solid lines within the shaded region represent the mean, which represents the average value across all simulations. **(A)** No change to any IL-2 specific parameters. **(B)** Parameter $\mathbf{j_{KO}}$ is increased by 300%. **(C)** Half rate suppression, K_{AKO} , is reduced by 83%; increasing the suppression strength of $\boldsymbol{\beta}$ in the IL-2 KO model by the same proportion.

3.8 Mathematical modeling code

All code scripts can be in the Hoyer lab box folder, my GitHub account (https://github.com/J-Anzules/HomeostaticExpansion), and if necessary, through e-mail (jonanzule@gmail.com).

Core Scripts

- **ModelandCellGrowth.m**
    - **Input**: Manual entry of parameter ranges
    - **Purpose**: Given the parameter range, it randomly chooses a value within the range, it sets up all the necessary conditions to run fmincon. Fmincon is the main driver for optimizing my objective function. Defined more below.
    - **Output**: Parameter sets, along with error values, and are saved to a csv file
    - **Fmincon**: link, This function is part of the matlab toolbox, its used to find the minimum of a constrained nonlinear multivariable function. Minimum is determined by the iteration of the parameters ranges that spits back the result of my objective function (GrowthObjective.m; below)
- **GrowthObjective.m**
    - **Input**: The initial step of this function uses the randomized parameters determined by ModelandCellGrowth.m. Future steps in the minimization process use parameters chosen by fmincon. It searches until it finds the minimum values calculated by GrowthObjective.m
    - **Purpose:** This script uses the parameter set fed to it by fmincon, which is then passed to the “SimulateGrowth.m" function that uses ode15s to solve my system of ODE’s. The population values determined by SimulateGrowth.m are done for both the WT and IL-2 KO simulation. Then the error is calculated by comparing appropriate sub populations in the simulation result to the appropriate experimental data. Once all the calculations are done, fmincon then determines whether another parameter set should be tested. If it does, it chooses the right parameters to evaluate next, until it determines that it has found the minimum value.
    - **Output**: Returns the sum of relative errors generated by this script. Fmincon will try to optimize the parameters, within the bounds of the model's constraints, to find the minimum error value. When it has done that, fmincon will return two things to me: the final parameter set and the errors (WT error, KO error, and total error).
    - **Notes:**
        - When it comes to the percentage removal part of the code
- **SimulateGrowth.m**
    - **Input**: Parameter set and Genotype value
        - 1 = WildType
        - 2 = Knockout
    - **Purpose**: Creates an empty dataset for the simulation values to be saved in, for every time step. Parameter set and initial conditions are given to my “Growth.m” function by ode15s. It does this for every time step

    - **Output**: A dataset called “ModelData” which contains the results of the simulation for either the WT or the KO simulation.
    - **Ode15s:** Solves stiff differential equations. The equations that it solves is provided by the growth.m script
- **Growth.m**
    - **Input:** time step, initial conditions, parameter set, and genotype
    - **Purpose**: Calculate population dynamics during a given time step
    - **Output**: Population numbers to be saved in a data frame within “SimulateGrowth.m”

Latin Hypercube Sampling

- **LHSInitialConditions**
    - **Input**: Sample size, Percent change, parameter set selection, initial conditions to be tested, and time frame
    - **Purpose**: Sensitivity test of initial conditions by latin hypercube sampling of desired conditions. Test parameters are set by the user.
    - **Output:** A multidimensional dataset of latin hypercube sampling results that is statistically analyzed by “CalculateTheFillRanges.m”
    - **Dependent core scripts:**
        - SimulateGrowth.m
        - Growth.m
        - CalculateTheFillRanges.m
- **CalculateTheFillRanges.m**
    - **Input**: Results from LHS, max hours of simulation
    - **Purpose:** From the LHS results of every population, at every hour, this script calculates the mean, standard deviation, +/- 1 standard deviation, and the 10th/90th percentile of those values.
    - **Output:** The results are organized into a multidimensional array (Dataframe: StatsOfCells) that is fed to the *PlottingLHSResults.m.*
- **PlottingLHSResults.m**
    - **Input:** Dataframe: StatsOfCells, time frame
    - **Purpose:** Depending on the experiment I will get plots that show the mean, the filled in ranges of all the simulations that lie between the 10th and 90th percentile of the LHS results.
    - **Output:** Plots
- **LHSParameters:**
    - **Input**: Sample size, Percent change, parameter set selection, initial conditions to be tested
    - **Purpose**: Sensitivity test of initial conditions by latin hypercube sampling of desired conditions. Test parameter are set by user.
    - **Output:** Plots of the filled in ranges between the 10th and 90th percentile of all simulations performed with varied parameters.
    - **Dependent core scripts:**
        - SimulateGrowth.m

- Growth.m

References

1. J. Michael Stolley and Daniel J. Campbell. “A 33D1 + Dendritic Cell/Autoreactive CD4 + T Cell Circuit Maintains IL-2–Dependent Regulatory T Cells in the Spleen”. In: The Journal of Immunology 197.7 (2016), pp. 2635–2645. issn: 0022-1767. doi: 10.4049/jimmunol.1600974.
2. Katrina K. Hoyer et al. “Interleukin-2 in the development and control of inflammatory disease”. In: Immunological Reviews 226.1 (2008), pp. 19–28. issn: 01052896. doi: 10.1111/j.1600- 065X.2008.00697.
3. Setoguchi R, Hori S, Takahashi T, Sakaguchi S. Homeostatic maintenance of natural Foxp3(+) CD25(+) CD4(+) regulatory T cells by interleukin (IL)-2 and induction of autoimmune disease byIL-2 neutralization. J Exp Med. 2005; 201:723–735. [PubMed: 15753206]
4. Khailaie, Sahamoddin, et al. "A mathematical model of immune activation with a unified self-nonself concept." Frontiers in immunology 4 (2013): 474.
5. Nelson, Brad H. "IL-2, regulatory T cells, and tolerance." The Journal of Immunology 172.7 (2004): 3983-3988.
6. Tang, Q. et al. Visualizing regulatory T cell control of autoimmune responses in nonobese diabetic mice. Nature Immunol. 7, 83–92 (2006).
7. Tadokoro, C. E. et al. Regulatory T cells inhibit stable contacts between CD4+ T cells and dendritic cells in vivo. J. Exp. Med. 203, 505–511 (2006).
8. Grossman, W. J. et al. Differential expression of granzymes A and B in human cytotoxic lymphocyte subsets and T regulatory cells. Blood 104, 2840–2848 (2004).
9. McHugh, R. S. et al. CD4+ CD25+ immunoregulatory T cells: gene expression analysis reveals a functional role for the glucocorticoid-induced TNF receptor. Immunity 16, 311–323 (2002).
10. Gondek, D. C., Lu, L. F., Quezada, S. A., Sakaguchi, S. & Noelle, R. J. Cutting edge: contact-mediated suppression by CD4+ CD25+ regulatory cells involves a granzyme B-dependent, perforin-independent mechanism. J. Immunol. 174, 1783–1786 (2005).
11. Chaudhry, Ashutosh, et al. "Interleukin-10 signaling in regulatory T cells is required for suppression of Th17 cell-mediated inflammation." Immunity 34.4 (2011): 566-578.
12. Xia, Jinxing, et al. "IL-15 promotes regulatory T cell function and protects against diabetes development in NK-depleted NOD mice." Clinical immunology 134.2 (2010): 130-139.
13. Johnson, M. L., & Faunt, L. M. (1992). [1] Parameter estimation by least-squares methods. In *Methods in enzymology* (Vol. 210, pp. 1-37). Academic Press.
14. Shampine, L. F. and M. W. Reichelt, “The MATLAB ODE Suite,” SIAM Journal on Scientific Computing, Vol. 18, 1997, pp. 1–22.
15. Shampine, L. F., M. W. Reichelt, and J.A. Kierzenka, “Solving Index-1 DAEs in MATLAB and Simulink,” SIAM Review, Vol. 41, 1999, pp. 538–552.
16. Khoruts, A., & Fraser, J. M. (2005). A causal link between lymphopenia and autoimmunity. *Immunology letters*, *98*(1), 23-31.
17. Moon, J. J., Chu, H. H., Pepper, M., McSorley, S. J., Jameson, S. C., Kedl, R. M., & Jenkins, M. K. (2007). Naive CD4+ T cell frequency varies for different epitopes and predicts repertoire diversity and response magnitude. Immunity, 27(2), 203-213.

18. Pedro Milanez-Almeida et al. “Foxp3+ regulatory T-cell homeostasis quantitatively differs in murine peripheral lymph nodes and spleen”. In: European Journal of Immunology 45.1 (2015), pp. 153–166. issn: 15214141. doi: 10.1002/eji.201444480
19. Janine Suffner et al. “Dendritic Cells Support Homeostatic Expansion of Foxp3 + Regulatory T Cells in Foxp3.LuciDTR Mice”. In: The Journal of Immunology 184.4 (2010), pp. 1810–1820. issn: 0022-1767. doi: 10.4049/jimmunol.0902420.
20. Rik Blok (2022). lhsdesigncon (https://github.com/rikblok/matlab-lhsdesigncon), GitHub. Retrieved September 9, 2022.
21. Malek, T. R., & Castro, I. (2010). Interleukin-2 receptor signaling: at the interface between tolerance and immunity. Immunity, 33(2), 153-165.
22. Lotze, M. T., Matory, Y. L., Ettinghausen, S. E., Rayner, A. A., Sharrow, S. O., Seipp, C. A., ... & Rosenberg, S. A. (1985). In vivo administration of purified human interleukin 2. II. Half life, immunologic effects, and expansion of peripheral lymphoid cells in vivo with recombinant IL 2. The Journal of Immunology, 135(4), 2865-2875.
23. Konrad, M. W., Hemstreet, G., Hersh, E. M., Mansell, P. W., Mertelsmann, R., Kolitz, J. E., & Bradley, E. C. (1990). Pharmacokinetics of recombinant interleukin 2 in humans. Cancer research, 50(7), 2009-2017
24. Schmidt, A., Oberle, N., & Krammer, P. H. (2012). Molecular mechanisms of treg-mediated T cell suppression. Frontiers in immunology, 3, 51.
25. Busse, Dorothea, et al. "Competing feedback loops shape IL-2 signaling between helper and regulatory T lymphocytes in cellular microenvironments." Proceedings of the National Academy of Sciences 107.7 (2010): 3058-3063.
26. Carneiro, J., Leon, K., Caramalho, Í., Van Den Dool, C., Gardner, R., Oliveira, V., ... & Demengeot, J. (2007). When three is not a crowd: a crossregulation model of the dynamics and repertoire selection of regulatory CD4+ T cells. *Immunological reviews*, *216*(1), 48-68.
27. Höfer, Thomas, Oleg Krichevsky, and Grégoire Altan-Bonnet. "Competition for IL-2 between regulatory and effector T cells to chisel immune responses." Frontiers in immunology 3 (2012): 268.

Chapter 4:

Summary, Contribution, Future Directions

4.1 Discussion

IL-2 cytokine determines the size, homeostasis, expansion, and function of Tregs. As evidenced by the IL-2 KO mouse model and patients with system lupus erythematosus, disruption of IL-2 cytokine functionality can result in the development of autoimmune disease [1]. However, due to the short half-life of IL-2 (30 min) [3, 4], it is challenging to experimentally track how IL-2 influences the entire system, specifically its maintenance of self-tolerance via Tregs. Using the mathematical model, I can study the dynamics of IL-2 and Tregs in preventing autoimmune disease and identify dysregulation that occurs before its onset.

I used experimental data to quantify various cellular populations from WT and IL-2 KO mouse models and observed the resulting differences and similarities. Using the least-squares method and the data collected, then I estimated the parameters of the mathematical model. As a result, I successfully captured the over-activation in the IL-2 KO data relative to the WT. With parameter ranges identified, I can further explore the dynamics of early immune dysregulation that may lead to autoimmune disease development.

Khailaie et al. noticed in their mathematical model that the renewal rate of naïve T cells could determine the activation threshold of the immune system [5]. Therefore, carefully controlling this rate and population can help differentiate between self- and non-self immune responses. In my mathematical model, I discovered that the production rate of naïve T cells from the thymus (mu) is the most sensitive parameter. Additionally, by the end of the simulation (day 18), there were more naïve T cells in the WT simulation than in the KO. These findings imply that the dynamics and homeostasis of the naïve T cell population can influence the susceptibility to autoimmune diseases. A more in-depth examination of naïve T cell homeostatic dynamics concerning autoimmune illness could provide additional insight.

I anticipated that the Treg population would be fewer in the IL-2 KO simulation because the absence of IL-2 cytokine increases their mortality rate; I did not anticipate, however, that the proliferation rate of Tregs would also be lower. Using Latin hypercube sampling, I examined the consistency of this pattern by conducting additional simulations with varying parameters associated with the death of Tregs; the pattern of increased Treg mortality and a lower Treg proliferation rate was constant despite the variations. Treg population in the IL-2 KO was consistently lower in all simulations. The mathematical model predicts that the Treg population in the IL-2 KO mouse model from birth has a greater mortality rate and a lower proliferation rate. The elevated death rate is consistent with the experimental findings of the Treg population without IL-2 [6, 8].

A greater Treg mortality rate, which may limit the quantity of Treg cells available for proliferation, might explain the lowered population size in the KO simulations. Based on my results, early peripheral Tregs (prior to day three) are likely to be the most impacted by IL-2 cytokine deficiency, since BALB/c mice begin to generate thymic Tregs robustly after day three

[9]. Future studies in the IL-2 KO should focus on early peripheral Tregs to better understand the immune dysregulation that occurs prior to the onset of autoimmunity.

I discovered that Treg inhibition of the activation rate of naïve T cells considerably reduces the development of autoimmunity in my simulations; these findings highlight the modulatory role that Tregs have on dendritic cells [10-14]. Furthermore, my results are supported by previous research showing that inoculating IL-2 cytokine into autoimmune mice improves Treg suppressive function, preventing autoimmunity [15]. Several clinical investigations have shown that low-dose IL-2 grows Tregs selectively and is safe and effective for patients with autoimmunity or graft-versus-host disease [28-32].

In contrast, deactivation of activated T cells by Tregs is insignificant for the prevention of autoimmunity; these results could be due to the absence of CD8 T cells. I hypothesize that the deactivation of activated T cells by CD8 T cells may compensate for the limited deactivation effect of Tregs [21]. Future iterations of themodel should incorporate the CD8 T cell population and their cytotoxic effect on activated T cells to assess this theory.

It is challenging to investigate the pathophysiology of autoimmune disease, even though risk factors and disease dynamics are known. My simulation can detect early immune dysregulation in the Treg population and prevent autoimmune disease through the manipulation of the suppressive ability of Tregs. These findings are consistent with experimental results. My mathematical model can serve to understand the deregulatory properties that occur before autoimmune disease can develop. Finally, minor changes to the structure of the mathematical model can be adapted to represent other autoimmune mouse models like CD25 knockout and scurfy mice models [28, 29].

4.2 Future Steps

Two projects can be pursued with no changes to the current mathematical model: determining the time point when an increased Treg suppression strength cannot prevent AD, and how many WT Tregs should be added to the IL-2 KO simulation to prevent AD. In addition, implementing the CD8 T cell population and its cytotoxic effect on the autoreactive CD4 T cell population would change the architecture of the mathematical model. However, it would give insight into the CD8 T cell influence on autoreactive T cells.

Implementation of CD8 T cells

The addition of the CD8 T cell population should have a structure comparable to that of the CD4 T cells already in my mathematical model structure, where a naive CD8 T cell population has an activation rate corresponding to an activated CD8 T cell population. For example, the population of CD8 T cells may be represented using the following equations:

Equation for naïve CD8 T cells

$$\frac{dE}{dt} = \epsilon E\left(1 - \frac{E}{K_E}\right) + S_E E - \theta E / \left(1 + \left(R\left(\frac{I}{K_E + I}\right)/K_B\right)\right) - d_E E$$

The equation for activated CD8 T cells

$$\frac{dC}{dt} = \theta E / \left(1 + \left(R\left(\frac{I}{K_E + I}\right)/K_B\right)\right) + S_C C - d_C C$$

Their cytotoxic activity on the activated CD4 T cell population will be represented by the term $j_C RC$ in the equation:

$$\frac{\mathrm{dT}}{\mathrm{dt}} = \beta \mathrm{N} / \left(1 + (\mathrm{R}\left(\frac{\mathrm{I}}{\mathrm{K_i} + \mathrm{I}}\right) / \mathrm{K_A})^{\mathrm{n}}\right) + \mathrm{s_T T} - \mathrm{jRT}\left(\frac{\mathrm{I}}{\mathrm{K_j} + \mathrm{I}}\right) - j_C RC - \mathrm{d_T T}$$

Further analysis for the prevention of autoimmune disease

In my simulations, I discovered that enhancing the suppressive capabilities of Tregs can prevent AD. However, I implemented the suppression modification at the start of the simulation run and predicting when it will be too late to take preventative actions would be an intriguing area of study. I propose automating the search by adding a failure condition to the algorithm. This requirement should be a threshold of 120% of the activated T cell population size in the KO simulation relative to the WT. With a failure condition in place, AD prevention can automatically be evaluated hourly without visual determination. The algorithm will reduce the K_A value every hour until it finds an hour when activated T cells in the KO simulation reach the failure condition.

In addition, the simulations may be further assessed to determine the number of healthy Tregs required to rescue the autoimmune simulation. For example, the IL-2 cytokine present in the WT simulation would influence the injected Tregs in the KO simulation, granting them enhanced survivability and function. In other experimental labs, an autoimmune mouse model has been rescued by the inoculation of healthy Tregs [22]. Finding out how many Tregs are necessary at various periods to rescue an autoimmune system will yield interesting results.

4.3 Limitations and Corrections

Although my simulations captured the over-activation seen in the KO data, the activated T cell simulation in WT did not fit the WT data well. Despite all the parameter variations, no set could simultaneously fit this WT data and display the over-activation in the KO simulation. My model's current structure does not represent the data collected. In this section, I will propose changes to the mathematical model that may improve the representation of activated T cells.

Activated T cells

During the model development, I assumed that all activated T cells produce IL-2 cytokine. However, activated T cells only generate IL-2 cytokines temporarily after activation [23]. In addition to IL-2's influence on Tregs, IL-2 also contributes to the proliferative rate of activated T cells [24]. Therefore, I should make two changes to represent activated T cell dynamics more

accurately:

1. To simulate more accurate immunological dynamics, create two distinct populations of activated T cells: one which generates IL-2 cytokine and another that does not .
2. Allow Il-2 cytokine to promote the proliferative rate of activated T cells

These modifications to the active T cell population may rectify the situation where the total activated T cells in the WT simulation do not accurately mimic the experimental data. The benefit of these modifications is that I will not require further data collection. I collected data on CD4 T cells undergoing early activation (CD4+CD69+) and activated T cells past early activation (CD4+CD44+CD62L-CD69-).

Naïve T cells

The naïve T cell repertoire may be dysregulated in pre-autoimmune systems because KO simulations have fewer naive T cells than WT. The experimental data showed that naïve T cells do not vary across genotypes. Hence, the models do not accurately depict the homeostatic components of the population. IL-7 is a known survival signal that maintains homeostasis and prolongs the lifespan of naive T cells [25]. Future model structures should establish a dynamic environment regulated by IL-7 cytokine. For example, any naive T cell population decline would increase the population's renewal rate until it reaches its homeostatic level.

Improved quantification of thymic output

I estimated the thymic contribution to the cellular populations based on the percentage of T cells detected in the thymus. For instance, if there are 5% Tregs in the thymus, I assumed 5% of Tregs in the spleen originated in the thymus. These assumptions may not be accurate, but it was a reasonable approximation. Future data collection efforts should aim to quantify T-cell receptor excision circles in Tregs and naive T cells to understand better the thymic contribution to these cellular populations [26, 27].

Conclusion

Despite the limitations of the simulations, it still offers a novel method for understanding homeostatic expansion in healthy and autoimmune systems. With the modifications outlined in this chapter, the mathematical model can offer far more insight into the dynamics of autoimmune disease. The methodology laid out here, along with adaptations of my mathematical model, may serve to describe other autoimmune mouse models (CD25 Knockout and scurfy mice).

References

1. Lieberman, L. A., & Tsokos, G. C. (2010). The IL-2 defect in systemic lupus erythematosus disease has an expansive effect on host immunity. *Journal of Biomedicine and Biotechnology*, *2010*.
2. Malek, T. R., & Castro, I. (2010). Interleukin-2 receptor signaling: at the interface between tolerance and immunity. Immunity, 33(2), 153-165.
3. Lotze, M. T., Matory, Y. L., Ettinghausen, S. E., Rayner, A. A., Sharrow, S. O., Seipp, C. A., ... & Rosenberg, S. A. (1985). In vivo administration of purified human interleukin 2. II. Half life, immunologic effects, and expansion of peripheral lymphoid cells in vivo with recombinant IL 2. The Journal of Immunology, 135(4), 2865-2875.
4. Konrad, M. W., Hemstreet, G., Hersh, E. M., Mansell, P. W., Mertelsmann, R., Kolitz, J. E., & Bradley, E. C. (1990). Pharmacokinetics of recombinant interleukin 2 in humans. Cancer research, 50(7), 2009-2017
5. Khailaie, Sahamoddin, et al. "A mathematical model of immune activation with a unified self-nonself concept." Frontiers in immunology 4 (2013): 474.
6. de la Rosa, M., Rutz, S., Dorninger, H., Scheffold, A. (2004) Interleukin-2is essential for CD4+CD25+ regulatory T cell function.Eur. J. Immunol.34,2480 -2488.5.
7. Furtado, G. C., Curotto de Lafaille, M. A., Kutchukhidze, N., Lafaille, J. J.(2002) Interleukin 2 signaling is required for CD4(+) regulatory T cellfunction.J. Exp. Med.196,851- 857
8. Fan, M. Y., Low, J. S., Tanimine, N., Finn, K. K., Priyadharshini, B., Germana, S. K., ... & Turka, L. A. (2018). Differential roles of IL-2 signaling in developing versus mature Tregs. Cell reports, 25(5), 1204-1213.
9. Asano, M., Toda, M., Sakaguchi, N., & Sakaguchi, S. (1996). Autoimmune disease as a consequence of developmental abnormality of a T cell subpopulation. *The Journal of experimental medicine*, *184*(2), 387-396.
10. Misra N, Bayry J, Lacroix-Desmazes S, Kazatchkine MD, Kaveri SV. Cutting edge: Human CD4+ CD25+ T cells restrain the maturation and antigen-presenting function of dendritic cells. J Immunol 2004;172:4676—80.
11. Houot R, Perrot I, Garcia E, Durand ILebecque S. Human CD4+ CD25 high regulatory T cells modulate myeloid but not plasmacytoid dendritic cells activation. J Immunol 2006;176: 5293—8.
12. Veldhoen M, Moncrieffe H, Hocking RJ, Atkins CJ, Stockinger B. Modulation of dendritic cell function by naive and regulatory CD4 + T cells. J Immunol 2006;176:6202—10.
13. Lewkowich IP, Herman NS, Schleifer KW, Dance MP, Chen BL, Dienger KM, et al. CD4+ CD25+ T cells protect against experimentally induced asthma and alter pulmonary dendritic cell phenotype and function. J Exp Med 2005;202: 1549—61
14. Serra P, Amrani A, Yamanouchi J, Han B, Thiessen S, Utsugi T, et al. CD40 ligation releases immature dendritic cells from the control of regulatory CD4+ CD25+ T cells. Immunity 2003;19:877—89.
15. Grinberg-Bleyer, Yenkel, et al. "IL-2 reverses established type 1 diabetes in NOD mice by a local effect on pancreatic regulatory T cells." Journal of Experimental Medicine 207.9 (2010): 1871-1878.
16. Koreth J, et al. (2011) Interleukin-2 and regulatory T cells in graft-versus-host disease. N Engl J Med365:2055–2066.13.
17. Long SA, et al.; Diabetes TrialNet and the Immune Tolerance Network (2012) Rapa-mycin/IL-2 combination therapy in patients with type 1 diabetes augments Tregs yet transiently impairsβ-cell function. Diabetes61:2340–2348.14.

18. Saadoun D, et al. (2011) Regulatory T-cell responses to low-dose interleukin-2 in HCV-induced vasculitis.N Engl J Med365:2067–2077.15.
19. He J, et al. (2016) Low-dose interleukin-2 treatment selectively modulates CD4(+)T cell subsets in patients with systemic lupus erythematosus.Nat Med22:991–993
20. Whitehouse, G., E. Gray, S. Mastoridis, E. Merritt, E. Kodela, J. H. M. Yang, R. Danger, M. Mairal, S. Christakoudi, J. J. Lozano, et al. 2017. IL-2 therapy restores regulatory T-cell dysfunction induced by calcineurin inhibitors. Proc. Natl. Acad. Sci. USA 114: 7083–7088.
21. Gravano, D. M., Al-Kuhlani, M., Davini, D., Sanders, P. D., Manilay, J. O., & Hoyer, K. K. (2016). CD8+ T cells drive autoimmune hematopoietic stem cell dysfunction and bone marrow failure. *Journal of autoimmunity*, *75*, 58-67.
22. Kim, J., Lahl, K., Hori, S., Loddenkemper, C., Chaudhry, A., deRoos, P., ... & Sparwasser, T. (2009). Cutting edge: depletion of Foxp3+ cells leads to induction of autoimmunity by specific ablation of regulatory T cells in genetically targeted mice. *The Journal of Immunology*, *183*(12), 7631-7634.
23. Sojka, D. K., Bruniquel, D., Schwartz, R. H., & Singh, N. J. (2004). IL-2 secretion by CD4+ T cells in vivo is rapid, transient, and influenced by TCR-specific competition. The Journal of Immunology, 172(10), 6136-6143.
24. Benczik, M., & Gaffen, S. L. (2004). The interleukin (IL)?2 family cytokines: survival and proliferation signaling pathways in T lymphocytes. Immunological investigations, 33(2), 109-142.
25. Rathmell, J. C., Farkash, E. A., Gao, W., & Thompson, C. B. (2001). IL-7 enhances the survival and maintains the size of naive T cells. *The Journal of Immunology*, *167*(12), 6869-6876.
26. Bains, I., Thiébaut, R., Yates, A. J., & Callard, R. (2009). Quantifying thymic export: combining models of naive T cell proliferation and TCR excision circle dynamics gives an explicit measure of thymic output. The Journal of Immunology, 183(7), 4329-4336.
27. Hazenberg, M. D., Otto, S. A., Stuart, J. W., Verschuren, M., Borleffs, J. C., Boucher, C. A., ... & Miedema, F. (2000). Increased cell division but not thymic dysfunction rapidly affects the T-cell receptor excision circle content of the naive T cell population in HIV-1 infection. Nature medicine, 6(9), 1036-1042.
28. Furtado, G. C., De Lafaille, M. A. C., Kutchukhidze, N., & Lafaille, J. J. (2002). Interleukin 2 signaling is required for CD4+ regulatory T cell function. *The Journal of experimental medicine*, *196*(6), 851-857.
29. Brunkow, M. E., Jeffery, E. W., Hjerrild, K. A., Paeper, B., Clark, L. B., Yasayko, S. A., ... & Ramsdell, F. (2001). Disruption of a new forkhead/winged-helix protein, scurfin, results in the fatal lymphoproliferative disorder of the scurfy mouse. *Nature genetics*, *27*(1), 68-73.